**Injection of a non-Newtonian fluid to improve the hydrofoil performance**

Mahya Hajihassanpour[1]

Jacobs, Leeds, UK

## Abstract

In this study, an active flow control method based on the injection of a non-Newtonian (NN) fluid through a slot on the suction side of a hydrofoil is proposed. The viscosity of several NN fluids including the Power-law, Carreau, Cross, Ellis, and Prandtl-Eyring are discussed and compared here. Besides NN fluids, the water as a Newtonian fluid is also employed in simulations to compare the efficiency of NN fluids against Newtonian ones. The governing equations are the two-phase Navier-Stokes equations that are numerically solved using the finite volume method with the Volume of Fluid (VoF) model to capture the interface of two fluids. This numerical solver used is examined by comparing its results with the experimental data for the fluid flow past NACA 0012 and NACA 0018 at the angles of attack $-4^{\circ} \leq \alpha \leq 26^{\circ}$, and Reynolds number is $Re_{\infty} = 3 \times 10^{6}$. This comparison shows that this numerical method used can reasonably compute the hydrofoil performance parameters including the lift coefficient, drag coefficient, and lift-to-drag ratio. When there is no injection, the water can be replaced with a NN fluid to figure out how changing the surrounding/primary fluid can affect the hydrodynamic performance of NACA 0012. In general, results indicate that the hydrofoil immersed in a NN fluid attains better performance. Moreover, while the surrounding fluid is assumed to be the water, the effect of injecting/blowing fluid which is either the water or NN fluid on the NACA 0012's performance is investigated here. Besides, the effect of momentum coefficients $C_m = 0.5$, 3.5, and 6.5 is also studied. Indications are that injection of the water is not a suitable way to improve the hydrodynamic performance of the hydrofoil at a moderate angle of attack. Furthermore, injection of the water at $C_m = 0.5$ is not suggested because the hydrofoil performance deteriorates, but at higher momentum coefficients like $C_m = 6.5$ the hydrofoil performance is improved at the stall point and beyond that. Contrary to the water case, the NN fluid is still effective for low momentum coefficient values. Indeed, the hydrofoil achieves better hydrodynamic performance for all the momentums coefficients in comparison with cases without the injection and injection of the water. The effect of the change of the NN fluid from the Carreau to the Prandtl-Eyring NN fluid is also examined, and conclusions are that the Prandtl-Eyring NN fluid is more successful in enhancing the hydrofoil performance and it can be preferred against Carreau fluid. Finally, the effect of the thickness of a hydrofoil on the efficiency of this active flow control method is studied. Observations indicate that injection of NN fluids can significantly improve the hydrodynamic performance of NACA 0012 and NACA 0018, however, it has much impact on the performance of a thicker hydrofoil which is NACA 0018 here. Therefore, this active flow control method based on injection of NN fluids is a reliable and effective method to mitigate unsteadiness, delay the stall, increase the lift coefficient, and decrease the drag coefficient, and finally, it can be considered as a suitable alternative method for other flow control techniques in hydrodynamic applications.

Keywords: Active flow control by the injection; Non-Newtonian fluid; Two-phase flow; Hydrofoil performance; Volume of Fluid (VOF) model

[1] mahya.hajihassanpour@jacobs.com

## 1. Introduction

There are many practical applications that a hydrofoil interacts with the liquid phase like the water, for example, pump impellers, tidal turbine blades, submarines, and marine propellers. Various flow conditions can occur in these applications, and for efficiently working in this wide range of flow conditions, usually exploiting a flow control technique is essential. The flow control methods can be classified into the passive and active methods. In the passive method, there is no need to consume energy to control the fluid flow, and desirable flow conditions can be achieved by modifying the original hydrofoil. For example, a flexible hydrofoil [1], slotted hydrofoil [2], Gurney flap [3], leading edge waviness [4], hydrofoil with dimple [5], leading edge slat [6], and vortex generators [7] are used in the literature to passively control the fluid flows in hydrodynamic applications. In contrast with the passive methods, in the active ones, energy consumption is needed to control/alter the fluid flow. While the passive methods are simple, the active ones can be suitably applied to precisely control the flow-field, and to finally achieve the defined design objects. Ventilation [8], liquid injection [9-13], suction [14], and synthesis jets [15] are examples of active flow control methods applied to hydrodynamic applications. Among these active flow control methods, the liquid injection [9-13] is suitable and easy to apply method, and this method is used here.

While it is well known in the literature that employing non-Newtonian fluids can effectively reduce the drag force and the pressure loss in internal flows [16-18], but its usage in external fluid flows is not finely studied. Specifically, using non-Newtonian fluids for controlling fluid flows past a hydrofoil is rarely studied in the literature. Chahine et al. [19] have used selective polymer injection to suppress cavitation emerging over a propeller. They have studied the effect of the additive polymer on the cavitation inception, torque, and thrust force. Their experimental work illustrated that injection of a polymer can be effective in delaying tip vortex cavitation inception. Here, we are going to use the injection of non-Newtonian fluids to control the flow-field characteristics around a hydrofoil, and to enhance its hydrodynamic performance. The lift and drag coefficients plus the lift-to-drag ratio are the performance parameters that are examined. Regarding flow-field characteristics, the streamlines, pressure, volume fraction, and viscosity are discussed. Different NN fluids are discussed in this study, such as the power-law [20, 21], Cross [22, 23], Carreau [24, 25], Ellis [24, 26], and the Prandtl-Eyring NN fluid rheology [27, 28]. Each NN fluid has its specific viscosity relation but the same density is assumed here. Moreover, the effects of the type of the surrounding/primary fluid, the momentum coefficient, the type of the injecting/blowing fluid, and the thickness of the hydrofoil are studied.

In this study, a non-Newtonian fluid will be injected into the water surrounded the hydrofoil. In this situation, a two-phase system should be simulated. The governing equations to model this two-phase flow are consist of a continuity equation and two viscous momentum equations plus an extra equation for the volume fraction of a fluid. Different numerical methods have been used in the literature to solve these governing equations and to capture the interface of two fluids [29, 30]. Here, the finite volume method with the implicit time discretization technique is used to solve the governing equations. Because the two fluids are not miscible, here the Compressive Interface Capturing Scheme for Arbitrary Meshes (CICSAM) [31, 32], which is essentially a Volume of Fluid (VOF) based method, is used to accurately capture the interface between two fluids.

This paper is organized as follows: The governing equations are given in Section 2. Definition of viscosity coefficients and different non-Newtonian fluids are presented in Section 3. Then, the numerical solver used in this study is discussed in Section 4. Results of simulations to examine the performance of the numerical

method used and to study the effectiveness of the proposed active control method are presented in Section 5. Finally, conclusions are given in Section 6.

## 2. Governing equations

Fluids concerned in this study are immiscible. Moreover, it is supposed that there is no mass transfer related to the cavitation phenomenon, and the weber number is sufficiently high so that the surface tension is neglected. Then, the governing equations can be written as:

$$\frac{\partial(\rho)}{\partial t} + \nabla \cdot (\rho \vec{u}) = 0 \tag{1}$$

$$\frac{\partial(\rho \vec{u})}{\partial t} + \nabla \cdot (\rho \vec{u}\vec{u}) = -\nabla p + \nabla \cdot \boldsymbol{\tau} \tag{2}$$

$$\frac{\partial(\phi_w)}{\partial t} + \nabla \cdot (\phi_w \vec{u}) = 0 \tag{3}$$

where $\rho$ indicated the mixture density, $\vec{u}$ is the velocity vector, and $p$ denotes the pressure. The volume fraction of the water and non-Newtonian fluids are indicated by $\phi_w$ and $\phi_{NN}$, respectively. Then, the mixture density can be calculated as follows:

$$\phi_w + \phi_{NN} = 1 \tag{4}$$

$$\rho = \rho_w \phi_w + \rho_{NN} \phi_{NN} \tag{5}$$

As to the shear stress tensor $\boldsymbol{\tau}$, it can be written as

$$\boldsymbol{\tau} = \mu \boldsymbol{D} \tag{6}$$

where $\boldsymbol{D}$ is the rate-of-deformation tensor.

## 3. Viscosity

The viscosity $\mu$ can be decomposed into the molecular/laminar $\mu_l$ and turbulent $\mu_t$ viscosities as follows:

$$\mu = \mu_l + \mu_t \tag{7}$$

$$\mu_l = \eta_w \phi_w + \eta_{NN} \phi_{NN} \tag{8}$$

In the case of the eddy/turbulent viscosity $\mu_t$, different turbulence models can be used to calculate it. Here, the Spalart-Allmaras turbulence model [33, 34] is used, because it can provide proper numerical results in external aerodynamic/hydrodynamic flows like the one concerning in the present study with a reasonable computational cost [35, 36]. The viscosity of the water as a Newtonian fluid is constant, and in the atmospheric condition, it is $\eta_w = 0.001003\ kg/ms$. However, the viscosity of the non-Newtonian fluid $\eta_{NN}$ is not constant like the water case.

Generally speaking, the non-Newtonian (NN) viscosity $\eta_{NN}$ depends on all three invariant of $\boldsymbol{D}$. Note that, from here onwards, to improve the readability, $\eta_{NN}$ is replaced with $\eta$. A series of NN fluids can be defined by considering $\eta$ as a function of the shear rate $\dot{\gamma}$ which is related to the second invariant of $\boldsymbol{D}$ by

$$\dot{\gamma} = \sqrt{\frac{1}{2}\boldsymbol{D}:\boldsymbol{D}} \tag{9}$$

Various NN fluids using $\eta(\dot{\gamma})$ have been proposed in the literature [26, 27, 37]. Among them, the power-law [20], Cross [22], Carreau [24, 25], and Ellis [24, 26] are popular ones that have been frequently used. The Prandtl-Eyring NN fluid rheology [27, 28] is also recently attracted the attention of researchers.

### 3.1. Power-law

This non-Newtonian fluid (NN) of Ostwald and de Waele [20] which is introduced in the 1920s can be written as

$$\eta(\dot{\gamma}) = \begin{cases} \eta_0, & \eta < \eta_0 \\ \eta_0 \dot{\gamma}^{n-1}, & \eta_0 \leq \eta \leq \eta_\infty \\ \eta_\infty, & \eta \geq \eta_\infty \end{cases} \tag{10}$$

where $\eta_\infty$ and $\eta_0$ are the predefined viscosities when the shear rate $\dot{\gamma}$ tends to infinite and to zero value, respectively. The viscosity at infinite shear rates can be rewritten as $\eta_\infty = K\eta_0$ where $K$ is a constant number. We are interested to recover the viscosity of water at low shear rates, so considering atmospheric conditions, we have $\eta_0 = 0.001003$. In the meantime, the viscosity of the NN fluid at high shear rates is preferred to be lower than the viscosity of water. Here, $K = 0.01$ is set. Regarding the power index $n$, while $n < 1$ represents NN fluids, utilizing $n = 1$ will give the water/Newtonian fluid. Here, $n = 0.4$ is used.

### 3.2. Cross fluid

Proposed by Cross in 1965 [22], the viscosity of this non-Newtonian fluid is expressed as follows:

$$\eta = \eta_\infty + \frac{\eta_0 - \eta_\infty}{1 + (B\dot{\gamma})^n} \tag{11}$$

where $n = 1$ and $B = 0.2$ are used here. Notice that by employing $n = 0$, the fluid behaves as a Newtonian liquid which is especially the water here.

### 3.3. Carreau fluid

This fluid has been introduced by Carreau in 1968 [24, 25], and has the following viscosity formula

$$\eta = \eta_\infty + (\eta_0 - \eta_\infty)(1 + (B\dot{\gamma})^2)^{\frac{n-1}{2}} \tag{12}$$

Here, $B = 0.5$ and $n = 0.2$ are used. While at low and high shear rates this fluid behaves as a Newtonian fluid with the viscosity $\eta_0$ and $\eta_\infty$, respectively, it behaves similar to a power-law fluid at intermediate shear rates. The Newtonian fluid with the viscosity $\eta_0$ can be obtained by setting $B = 0$.

### 3.4. Ellis fluid

The rheology of this non-Newtonian (NN) fluid is a bit different than the previously presented NN fluids. While in the power-law, Cross, and Carreau NN fluids the viscosity reaches a prescribed value at high shear rates, there is no prescribed value here. The viscosity of this NN fluid [24, 26] can be expressed as

$$\eta = \frac{\eta_0}{1 + \left(\frac{\dot{\gamma}}{\dot{\gamma}_{\frac{1}{2}}}\right)^{n-1}} \tag{13}$$

where $\dot{\gamma}_{\frac{1}{2}}$ is a predefined shear rate at which $\eta = \eta_0/2$. Using $n = 1$, the fluid behaves as a Newtonian fluid. Here, $n = 1.9$ and $\dot{\gamma}_{\frac{1}{2}} = 5$ are used.

### 3.5. Prandtl-Eyring fluid

Like the previously non-Newtonian (NN) fluids, this is also a shear-thinning fluid that introduced by Prandtl and Eyring in the 1930s [27, 28] and has the viscosity of

$$\eta = \begin{cases} \frac{A}{\dot{\gamma}}\left[\epsilon - \frac{\epsilon^3}{6} + \frac{3\epsilon^5}{40} - \frac{15\epsilon^7}{336} + \frac{105\epsilon^9}{3456} - \frac{945\epsilon^{11}}{42240}\right], & \epsilon < 1 \\ \frac{A}{\dot{\gamma}}\left[ln(2\epsilon) + \frac{1}{4\epsilon^2} - \frac{3}{32\epsilon^4} + \frac{15}{288\epsilon^6} - \frac{105}{3072\epsilon^8} + \frac{945}{38400\epsilon^{10}}\right], & \epsilon \geq 1 \end{cases} \tag{14}$$

with $\epsilon = \dot{\gamma}/B$ and $A = B\eta_0$. This NN fluid behaves like the Ellis fluid so that there is no constrain for high shear rates. Here, $B = 1$ is used, and employing high values result in having a Newtonian fluid with the viscosity $\eta = \eta_0$.

In Fig. 1., a comparison between these NN fluids has been made. Discontinuities in the viscosity profile of the power-law NN fluid may cause numerical difficulties such as deteriorating the solution convergence or degrading the solution accuracy. The viscosity profile of the Carreau and Cross NN fluids are similar. As depicted in Fig. 1, the Prandtl-Eyring and Ellis NN fluids also behave similarly. Thus, among these NN fluids, the Carreau and Prandtl-Eyring NN fluids are selected to perform simulations. Moreover, unless otherwise mentioned, all the simulations are performed by considering the Carreau as a NN fluid.

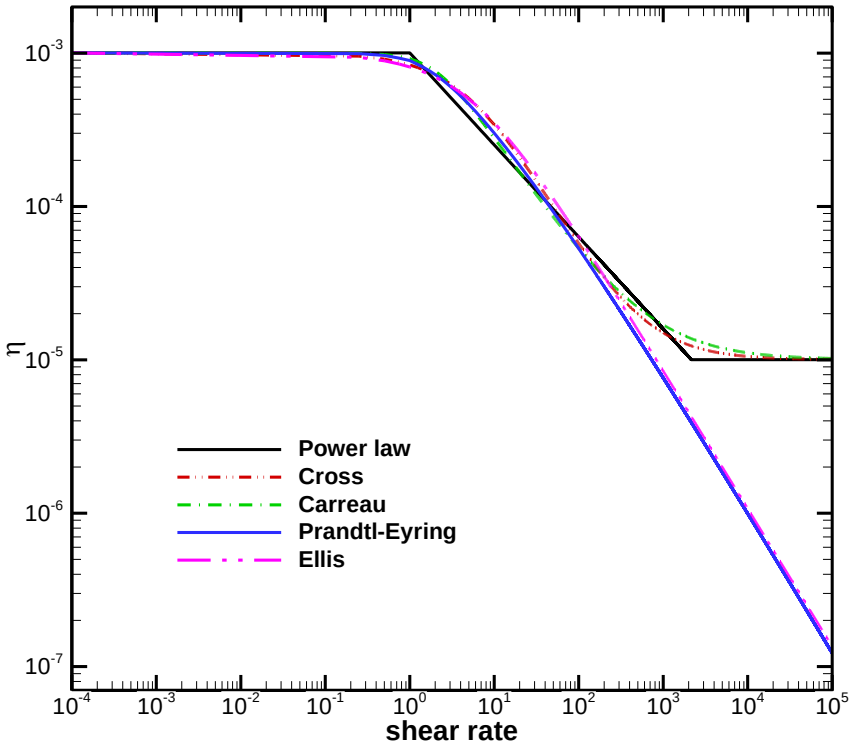


Fig. 1 Laminar/molecular viscosity coefficient computed for different non-Newtonian fluids.

## 4. Numerical solver

The finite volume method is used here to solve the governing equations (1)-(3). First of all, the pressure-velocity coupling problem arising in incompressible fluid flows is tackled using the SIMPLE scheme, and

for computing the pressure, the staggered-grid scheme is utilized. In the governing equations, the gradient operators are discretized using the Green-Gauss theorem with the arithmetic average of the nodal values on the faces. Then the numerical fluxes are computed using a second-order upwind scheme. The temporal derivative terms are also discretized by applying a first-order implicit method. Finally, a Volume of Fluid (VoF) based method which is the Compressive Interface Capturing Scheme for Arbitrary Meshes (CICSAM) [31] is used to sharply capture the interface between two fluids.

## 5. Results

In this study, the fluid at the far-field which is called the surrounding/primary fluid will be the water or a non-Newtonian fluid. The surrounding fluid is assumed to be incompressible with the density $\rho = 998.2\ kg/m^3$. Moreover, the Reynolds number is $Re_\infty = 3 \times 10^6$ which is high enough to consider the flow regimes as the turbulent flow. Then, the velocity magnitude $U_\infty$ can be straightforwardly obtained from the definition of the Reynolds number.

Regarding the hydrofoil, NACA 0012 or NACA 0018 with the chord length $c = 1$ will be used in simulations. A slot is placed at $x = 0.05$ over the upper surface of the hydrofoil and the water or non-Newtonian fluid injects through this slot at the angle of attack 20 degrees meaning it is tangentially injected over the surface. This injecting/blowing fluid is used to alert fluid flow characteristics past the hydrofoil to enhance its performance. Meanwhile, the slot width is assumed to be $h = 0.0035$, and the velocity of the injecting fluid $U_b$ can be calculated from the definition of the moment coefficient $C_m = 2hU_b^2/cU_\infty^2$. The hydrofoil and injecting fluid parameters are set based on the non-dimensionalization values proposed by Muller-Vahl and Greenblatt in [38]. They have shown that injection of the air can be useful to control the deep stall of an airfoil. Contrary to their work, here we are dealing with liquids, not gaseous fluids, so we will have a hydrofoil, not an airfoil. Furthermore, besides the water, we will also exploit the idea of using non-Newtonian fluids to enhance the hydrofoil performance.

### 5.1. Validation

To assess the accuracy of the numerical method, fluid flows past NACA 0012 and NACA 0018 hydrofoils are simulated, and numerical results are compared against the experimental data [34, 39-41]. Here, a grid with 76185 cells and 46418 nodes is used to discretize the solution domain. This generated grid is shown in Fig. 2 and it can be seen that a fine grid resolution is considered near the hydrofoil surface while a coarser one is generated far from it. Only the generated grid for NACA 0012 is shown in this figure. In the case of NACA 0018, a grid can be easily generated by scaling up the generated grid done for NACA 0012 in the $y$-direction exactly equals to their thickness ratio, i.e., $18/12 = 1.5$. The water flow, by setting $B = 0$ in Eq. (12) for the non-Newtonian Carreau fluid, is considered here. Thus, although we solve the two-phase governing equations, the simulation output will be a single-phase flow. The pressure contours with streamlines for different angles of attack are shown in Fig. 3. Generally, the pressure reaches its minimum value near the leading edge of the hydrofoil and on the suction side where the fluid accelerates causing the pressure drop. Owing to the presence of the adverse pressure gradient, the separation firstly appears on the suction side from the training edge, and it goes toward the leading edge at higher angles of attack. Basically, an attached vortex will be formed over the hydrofoil's surface at low or moderate angles of attack, but a vortex shedding will be formed at high angles of attack. The vortex shedding can be considered as a characteristic of the stall when the lift coefficient drops suddenly and the separation of the flow takes place near the leading edge. As indicated in this figure, NACA 0018 exhibits different flow pattern at the angles

of attack 22° and 26° in comparison with NACA 0012. While two large wall-attached vortices are formed over NACA 0018, the unsteady flow can be seen for NACA 0012 at these angles of attack. A graph of the lift coefficient versus the angle of attack is shown in Fig. 4. The stall for NACA 0018 gradually occurs, but it is sharp in the case of NACA 0012. The stall and post-stall flow characteristics are completely nonlinear phenomena and they strongly depend on the hydrofoil profile and Reynolds number. In fact, how much the size of the separation bubble formed on the hydrofoil is sensitive to variations of the angle of attack and how fast the boundary layer separation point moves toward the leading edge by increasing the angle of attack will affect the stall and post-stall flow characteristics. Comparison between obtained numerical results and the experimental data [34, 39-41] is presented in Fig. 4 that proves that the present numerical solver can provide reasonable results fitting appropriately with experimental data.

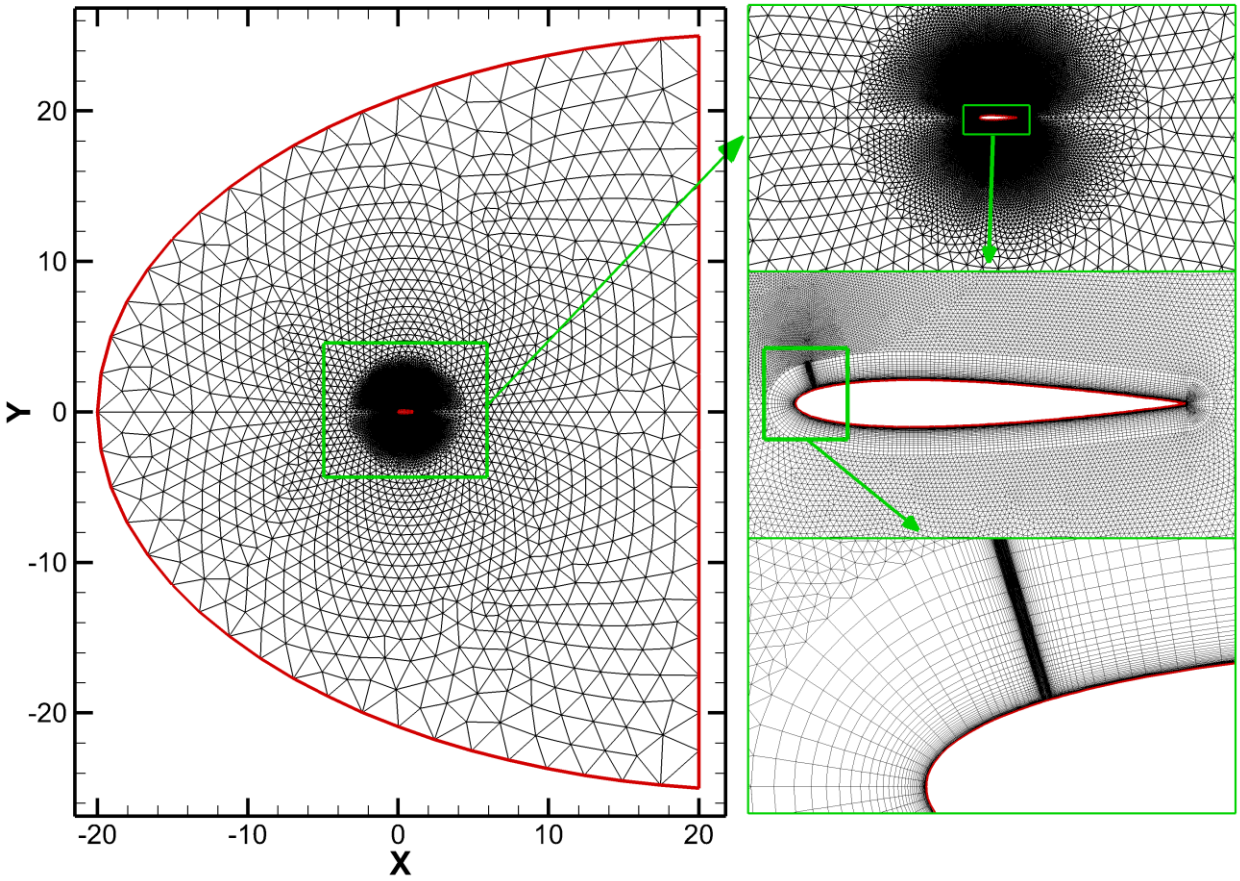


Fig. 2 Generated grid with 76185 cells and 46418 nodes.

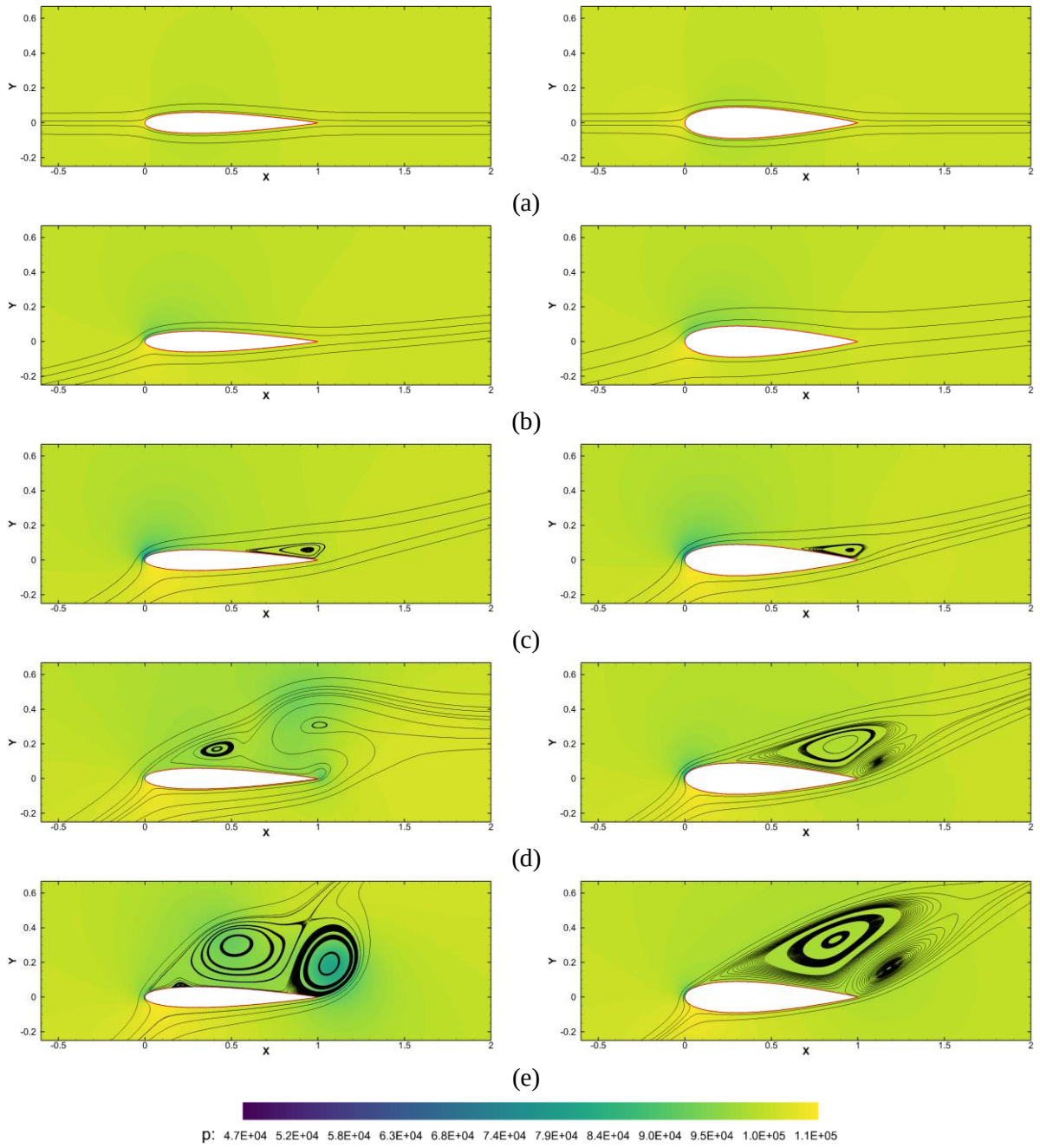


Fig. 3 Pressure contour with streamlines obtained for the water flow past NACA 0012 (Left column) and NACA 0018 (right column) at the angles of attack a) 0˚, b) 8˚, c)18˚, d) 22˚, and e) 26˚.

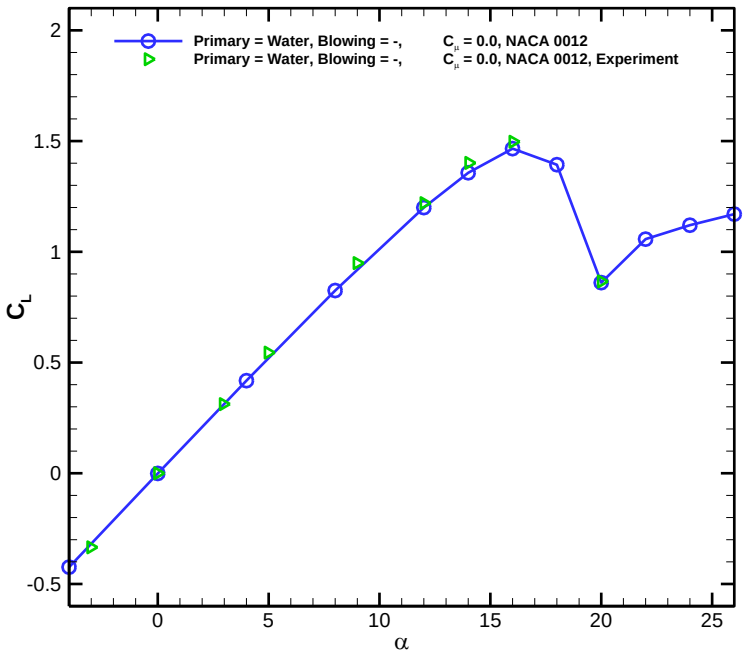


(a)

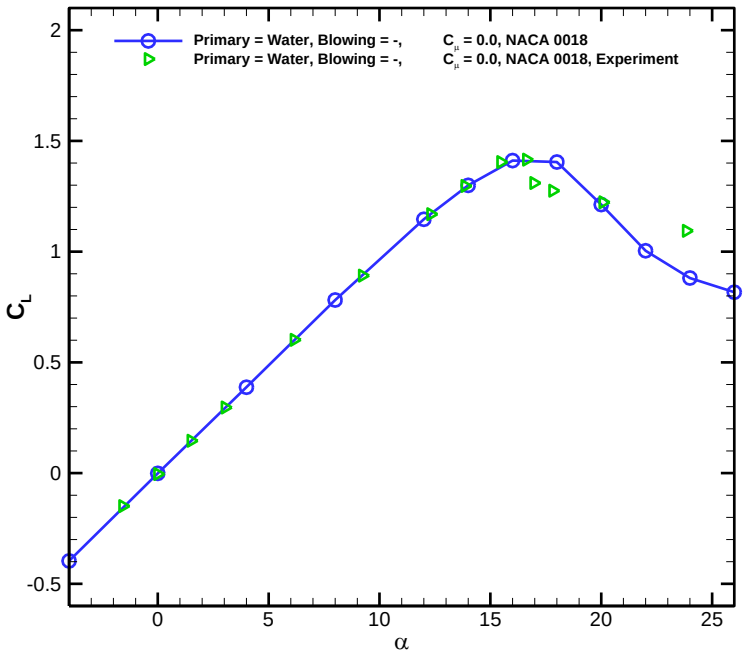


(b)

Fig. 4 The lift coefficient obtained for a) NACA 0012 and b) NACA 0018 hydrofoils.

### 5.2. Effect of the change of the surrounding fluid from the water to non-Newtonian fluid

While in Section 5.1 the surrounding/primary fluid was water, here the non-Newtonian (NN) Carreau fluid is used to figure out how the change of the surrounding fluid may affect flow characteristics past NACA 0012 hydrofoil. In Fig. 5, the pressure contours with streamlines and contours of the laminar/molecular viscosity have been shown. Despite using the water as a surrounding fluid resulting in appearing of unsteady vortices at $\alpha = 22^{\circ}$ (see Fig. 3), we have a small wall-attached vortex when the NN fluid is considered. However, similar to the water case, there is still a steep stall when the angle of attack increases from $22^{\circ}$ to $26^{\circ}$.

Computed molecular viscosity for this NN fluid flow shows that at the far-field, where there is no significant amount of the shear rate, the molecular viscosity remains constant and equals the water viscosity. However, near the hydrofoil wherein a larger amount of the shear rate can be expected, the molecular viscosity reduces dramatically resulting in magnifying inertial forces and reducing viscous forces. The fluid flow separates if the inertial force is not sufficient to provide a favorable pressure gradient, however, by employing the NN fluid, the inertial force will increase helping to mitigate the separated flow and to delay the stall. Comparison of Fig. 3(c) and Fig. 5(c) shows that at $\alpha = 18^{\circ}$ using the NN fluid will be useful to remove the separation bubble. This is achieved as a consequence of adding more kinetic energy to that region. Moreover, the separation from the leading edge is prohibited using the NN fluid at $\alpha = 22^{\circ}$. However, reduction in the viscous drag by utilizing the NN fluid at $\alpha = 26^{\circ}$ is not enough to prevent occurrence of the unsteady separation flow, and similar to the water case there is a vortex shedding. In the right column of Fig. 5, it can be seen that the molecular viscosity usually becomes minimum near the leading edge, the trailing edge, the borders of separated flow regions, and in the wake. These are regions with large amount of the shear rate.

In Fig. 6, the performance of the hydrofoil immersed in the NN fluid is compared with the water one. This comparison shows that the lift coefficient slope, maximum lift coefficient, and stall angle of attack (called also stall point) are favorably increased. While there is no significant change at low angles of attack, near the stall point the hydrofoil attains better performance in the NN fluid in comparison with the water one. For example, the difference between the lift coefficient at $\alpha = 20^{\circ}$ obtained for the NN and the water fluids is $\Delta C_l = C_{l_{NN}} - C_{l_w} \approx 1.85 - 0.85 \approx 1$. It means that by this active flow control method this new hydrofoil can achieve 2.2 times as many lift coefficients as the original hydrofoil. The drag reduction is even much more interesting. The drag coefficient, obtained when the NN fluid is used, is always lower than the water case. Moreover, the drag reduction is more significant near the stall point, for instance, at $\alpha = 22^{\circ}$ the drag reduction is $\Delta C_D = C_{D_{NN}} - C_{D_w} = 0.06 - 0.41 = -0.35$ which is about 1/6.84 of the drag coefficient of the original hydrofoil. When the NN fluid is used, the lift-to-drag ratio $L/D$ for all the angles of attack shows an improvement, however, at high angles of attack like $\alpha = 24^{\circ}$ or $26^{\circ}$ it loses its efficiency and there is no exclusive priority when the NN fluid is used instead of the water one.

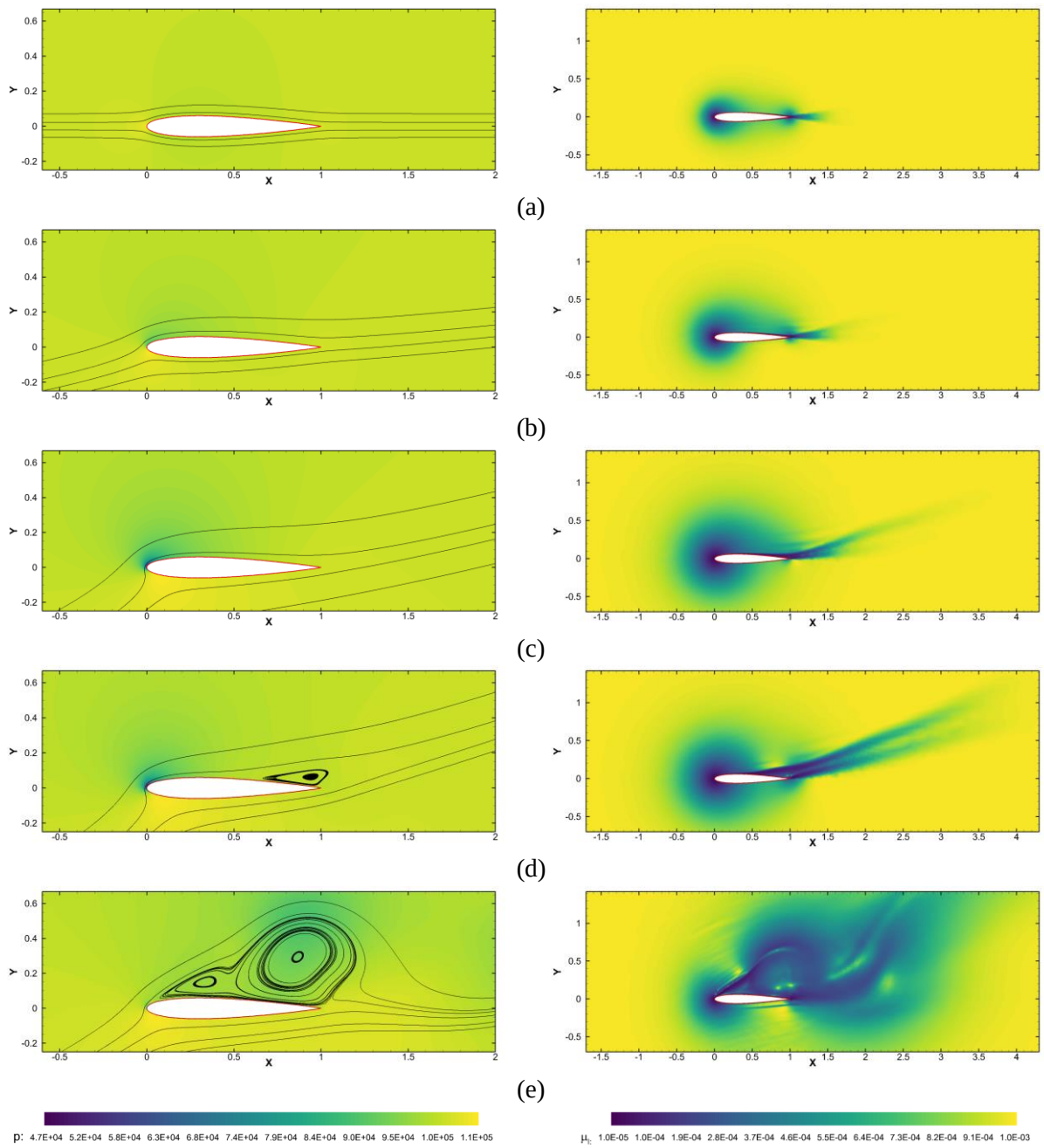


Fig. 5 Pressure contours with streamlines (left column) and molecular/laminar viscosity contours (right column) obtained for the non-Newtonian fluid flow past NACA 0012 hydrofoil at the angles of attack a) 0, b) 8, c)18, d) 22, and E) 26.

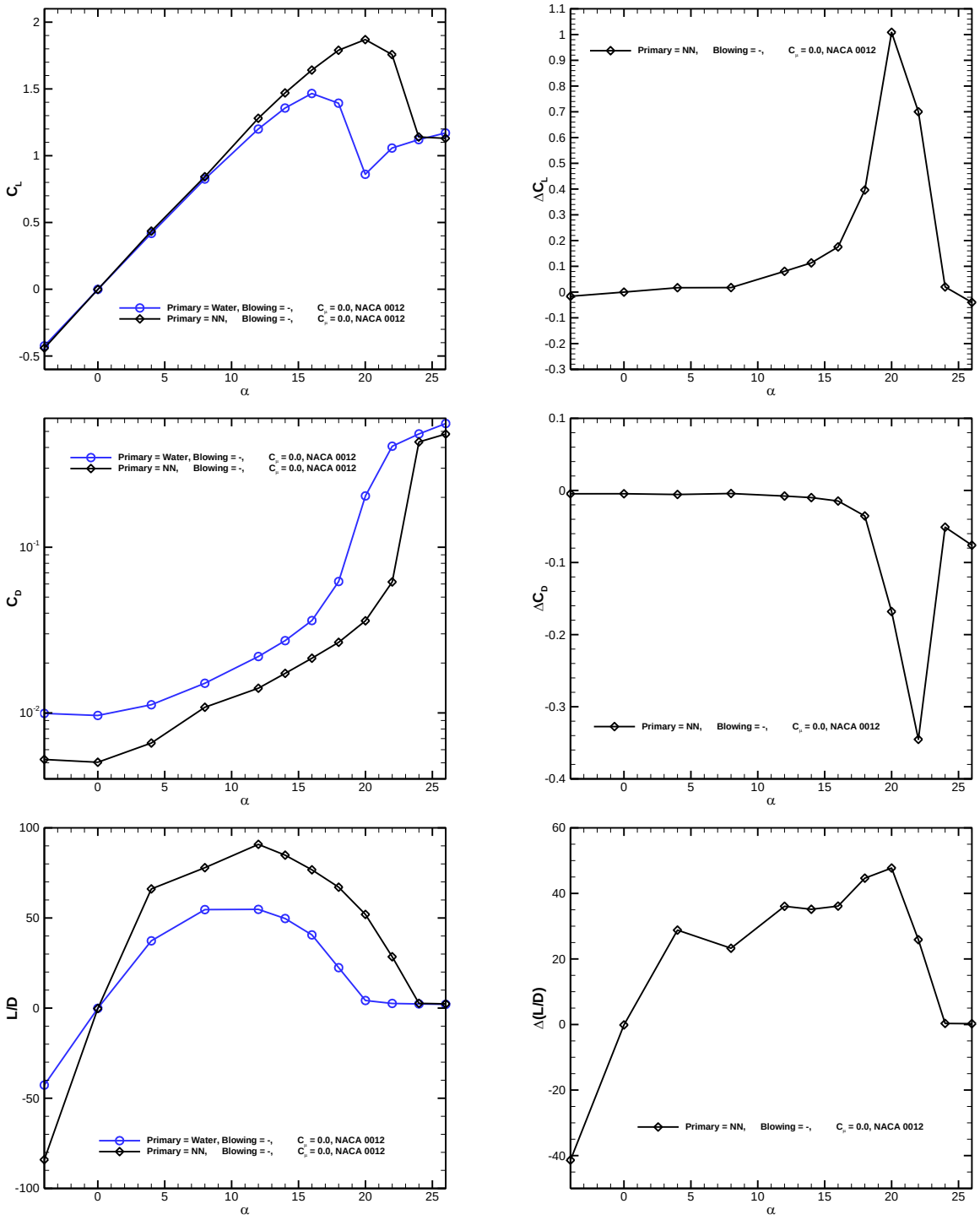


Fig. 6 Comparison of performance of NACA 0012 when it is immersed in a water medium versus when it is immersed in the non-Newtonian (NN) fluid.

### 5.3. Effect of the change of the injecting fluid from the water to non-Newtonian fluid

In this section, while the water (a Newtonian fluid) is considered as the surrounding/primary fluid, the water or NN fluid is injected through a slot placed on the suction side of NACA 0012 hydrofoil to investigate in details how changing the type of the injecting/blowing fluid will alter the flow characteristics and the hydrofoil performance. The non-Newtonian Carreau fluid is injected with three different momentum coefficients that are $C_m = 0.5, 3.5,$ and $6.5$. Increasing the momentum coefficient means the injection of a fluid with higher velocity levels. Changing this parameter helps to figure out how it may affect the flow characteristics and the hydrofoil performance as well.

The flow characteristics shown by the pressure contours with the streamlines and the volume fraction contours for $C_m = 0.5$ are illustrated in Fig. 7. When the water is injected through the slot, the flow remains steady until $\alpha = 18^{\circ}$ but it becomes unsteady at higher angles of attack such as $\alpha = 22^{\circ}$ or $26^{\circ}$. However, by injection of the NN fluid instead of the water, at $\alpha = 18^{\circ}$ the size of the wall-attached vortex becomes smaller and at $\alpha = 22^{\circ}$ the flow changes from an unsteady state to a steady one. However, it still remains unsteady at $\alpha = 26^{\circ}$ but with different flow patterns. It can be seen from the right column of Fig. 7 that the concentration of the NN fluid would be around the border of the separated flow regions. In the case of $\alpha = 22^{\circ}$, the separated flow region is filled out with the NN fluid.

In Fig. 8, the performance parameters including the lift coefficient, drag coefficient, and lift-to-drag ratio are presented. Investigation of the lift-to-drag ratio demonstrates that using the NN fluid results in a better performance in comparison with both situations without injection and injection of the water. When the water is served as the injecting fluid, then $L/D$ is deteriorated in comparison with the case of without injection until $\alpha = 18^{\circ}$, but succeeding that angle there is no significant improvement/deterioration. In the case of injection of the NN fluid, significant changes occur at $\alpha = 20^{\circ}$ and $22^{\circ}$. At $\alpha = 20^{\circ}$, the NN fluid preferably brings about higher lift coefficient levels and lower drag coefficient ones meaning better hydrofoil performance. However, at $\alpha = 22^{\circ}$, while the lift coefficient is undesirably lower than the one for the water case, the drag coefficient is desirably still lower resulting in a still better hydrodynamic performance for NACA 0012 hydrofoil.

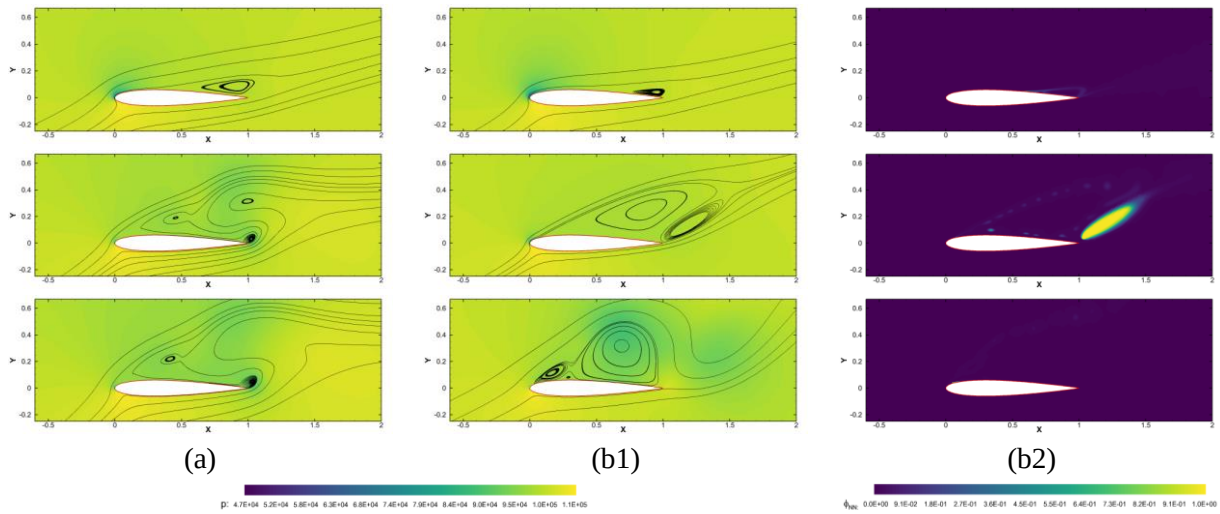


Fig. 7 Pressure contour with streamlines and contour of volume fraction of NN fluid for a) Water-water and b) water-NN fluid flows past NACA 0012 at the momentum coefficient 0.5 and angles of attack 18 (upper row), 22(middle row), and 26 (lower row).

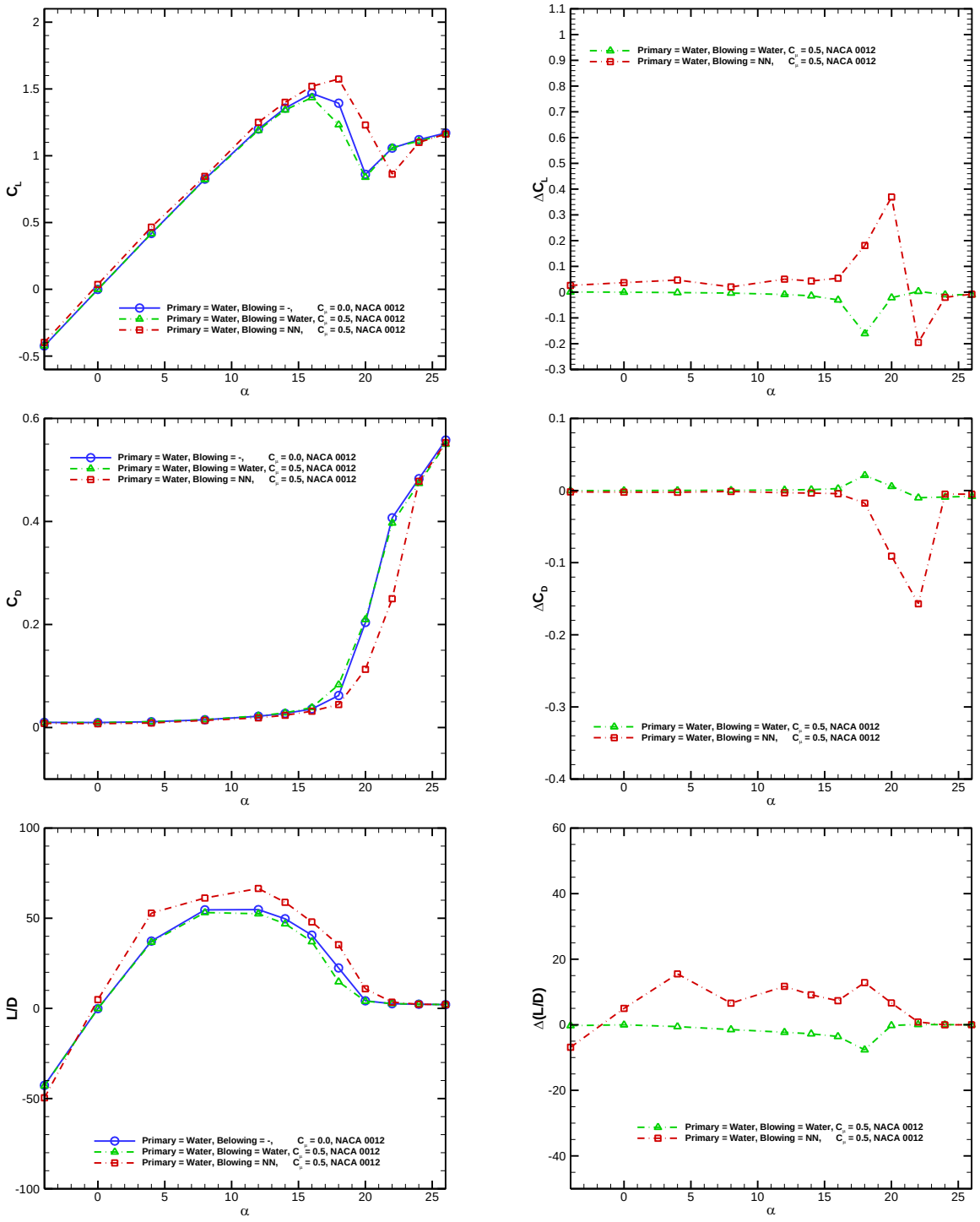


Fig. 8 Performance of NACA 0012 calculated at the momentum coefficient 0.5.

When the water is injected, it is illustrated in Fig. 9 that by increasing the momentum coefficient from $C_\mu =$ 0.5 to 3.5, the unsteady flow structures appear at $\alpha = 26^\circ$ instead of $22^\circ$. However, using the NN fluid gives steady flow condition until $\alpha = 26^\circ$. It means that using higher momentum coefficient might be helpful to delay the emergence of unsteady fluid flows and to prevent the boundary layer separation.

The hydrodynamic parameters obtained using $C_\mu = 3.5$ are given in Fig. 10. As indicated in this figure, in the case of the injection of the water, when there is a small separated flow region over the hydrofoil occurring at the angles of attack less than the stall one, while the lift force is not affected by the injection of the water the drag force is unappealingly increased. Note that at low angles of attack that there is a small separated flow region over the hydrofoil, the major portion of the total drag would be the friction drag, while at high angles of attack with a large separated flow region the pressure drag would be dominant. Injection of the water increases the shear force causing an increase in the friction drag. However, at higher angles of attack, the injection of the water can mitigate the size of the separated flow region and subsequently leads to a lower pressure drag and then finally lower the total drag. This is exactly why using the injection of the water will result in a better hydrofoil performance at higher angles of attack and deteriorate the hydrodynamic efficiency of the hydrofoil at lower ones. However, the NN fluid will have a lower viscosity coefficient in regions with higher shear stresses leading to lower friction force. In other words, by exploiting the NN fluid having a lower viscosity coefficient the viscous drag can be decreased, the extent of the separated flow region can be shrunk, and the pressure drag can be decreased. In general, the hydrofoil with the NN fluid attains higher lift-to-drag ratio in comparison with the hydrofoil with the injection of the water and without the injection.

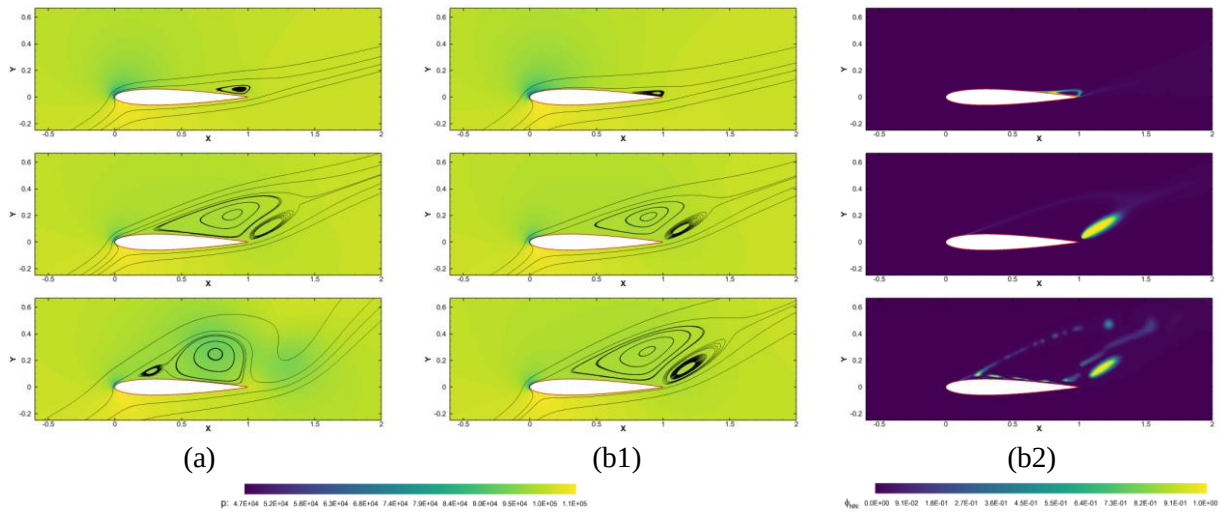


Fig. 9 Pressure contours with streamlines and volume fraction contours of the NN fluid for a) Water-water and b) water-NN fluid flows past NACA 0012 at the momentum coefficient 3.5 and angles of attack $18^\circ$ (upper row), $22^\circ$ (middle row), and $26^\circ$ (lower row).

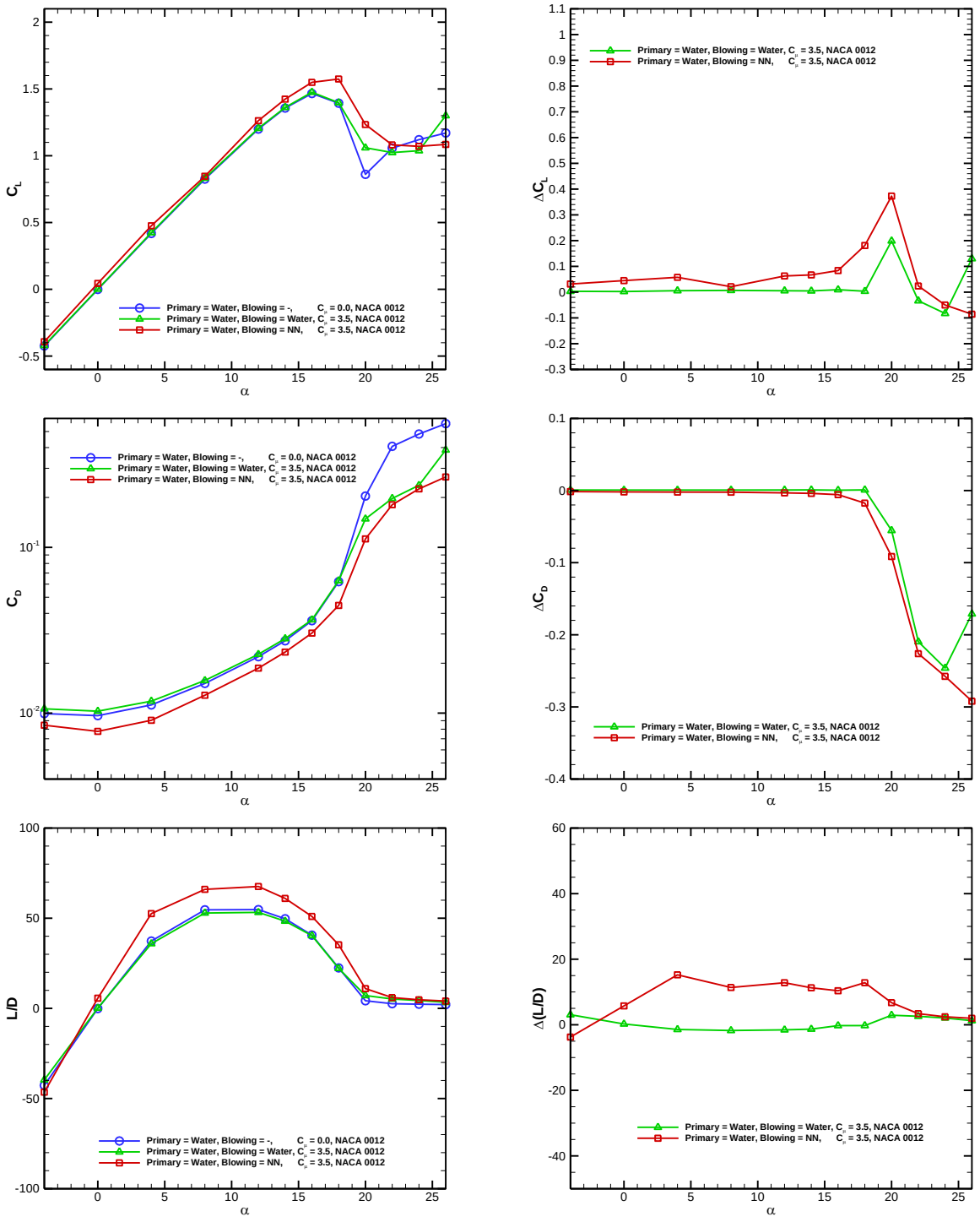


Fig. 10 Performance of NACA 0012 obtained for the momentum coefficient 3.5.

By increasing the momentum coefficient to $C_\mu = 6.5$, as indicated in Fig. 11, the flow remains steady-state up to $\alpha = 26^\circ$ for both cases of the injection of the water and the NN fluid. Regarding the hydrofoil performance, it is shown in Fig. 12 that always the NN fluid can result in higher lift-to-drag ratio, lower drag coefficient, and higher lift coefficient levels. As indicated in this figure, the most impact of the injection of the fluid would be changing the flow characteristics near the stall point, and essentially delaying the stall inception. Note that by utilizing the NN fluid we would be able to simultaneously decrease the drag and increase the lift in all the range of angles of attack.

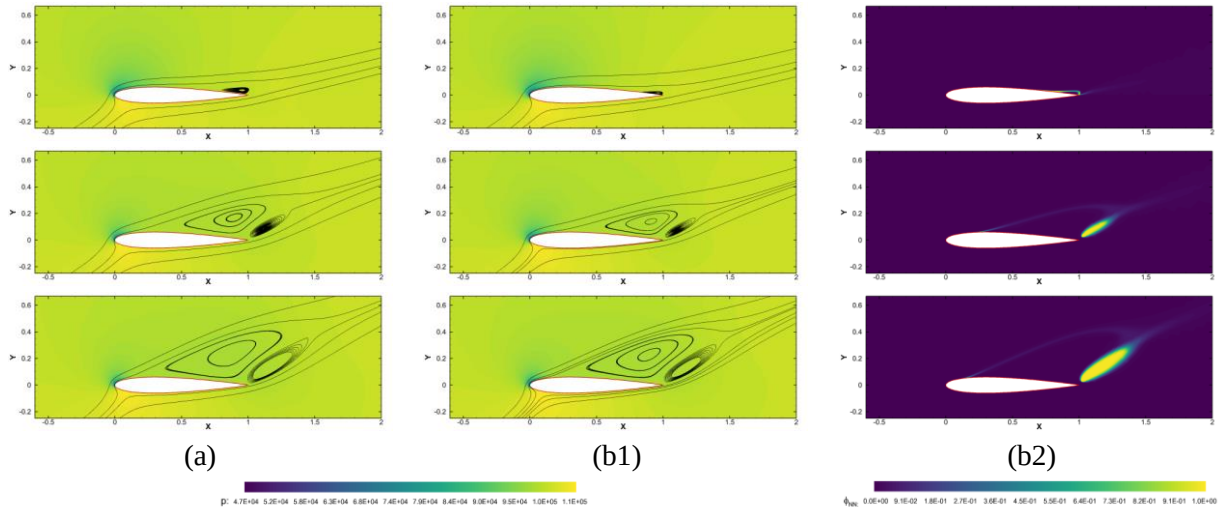


Fig. 11 Pressure contour with streamlines and contour of volume fraction of NN fluid for a) Water-water and b) water-NN fluid flows past NACA 0012 at the momentum coefficient 6.5 and angles of attack 18 (upper row), 22(middle row), and 26 (lower row).

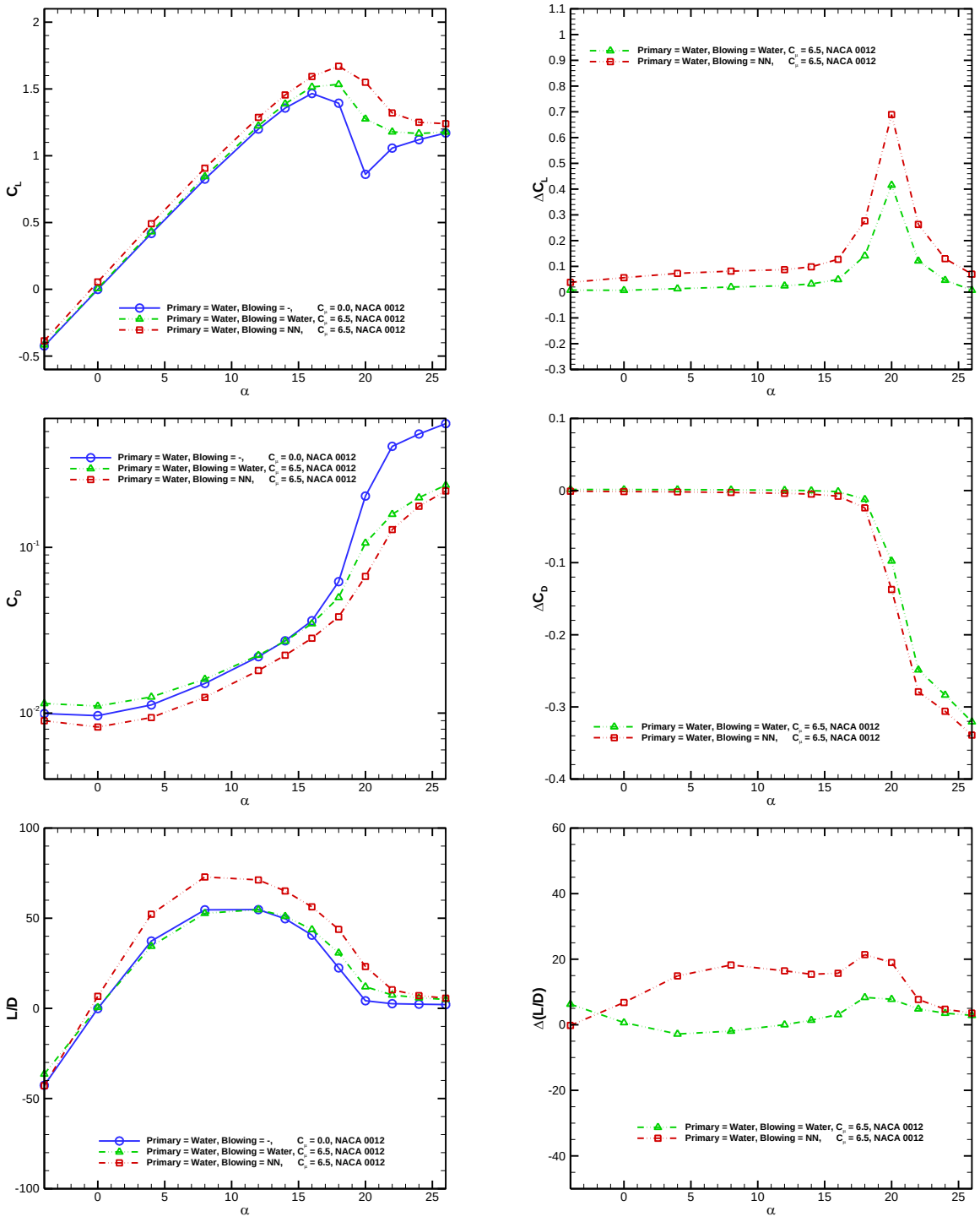


Fig. 12 Performance of NACA 0012 calculated at the momentum coefficient 6.5.

### 5.3.1. Effect of the momentum coefficient when the water is used as an injecting fluid

Indicated in Fig. 13 for the water case, using $C_\mu = 0.5$ not only is not useful but also it deteriorate the hydrofoil performances so that the lift coefficient is always lower and the drag coefficient is higher than those in the case of without injection. However, using $C_\mu = 6.5$ leads to attaining higher lift coefficients at all angles of attack and lower drag coefficients for $\alpha \geq 14^\circ$. In the case of $C_\mu = 3.5$, we experience an intermediate state between the two discussed momentum coefficients. Therefore, it can be concluded that for using the water as the injecting/blowing fluid, choosing higher momentum coefficients would be strongly recommended. In other words, using lower values should be avoided.

### 5.3.2. Effect of the momentum coefficient when the non-Newtonian fluid is used as an injecting fluid

It can be seen in Fig. 14 that in general increasing the momentum coefficient will improve the hydrofoil performances even for $C_\mu = 0.5$. It is in contrast with the water case that considering $C_\mu = 0.5$ causes degrading the lift-to-drag ratio. As indicated in this figure, investigation of the lift coefficient and the lift-to-drag ratio shows that there is no significant prominence for $C_\mu = 3.5$ over $C_\mu = 0.5$. However, by utilizing $C_\mu = 6.5$ all the performance parameters are meaningfully improved in comparison with $C_\mu = 3.5$ and $C_\mu = 0.5$. Thus, using low momentum coefficients would be beneficial to increase the lift coefficient, decrease the drag coefficient, delay the stall, and increase the lift-to-drag ratio. However, higher momentum coefficients can be employed to achieve still better performances.

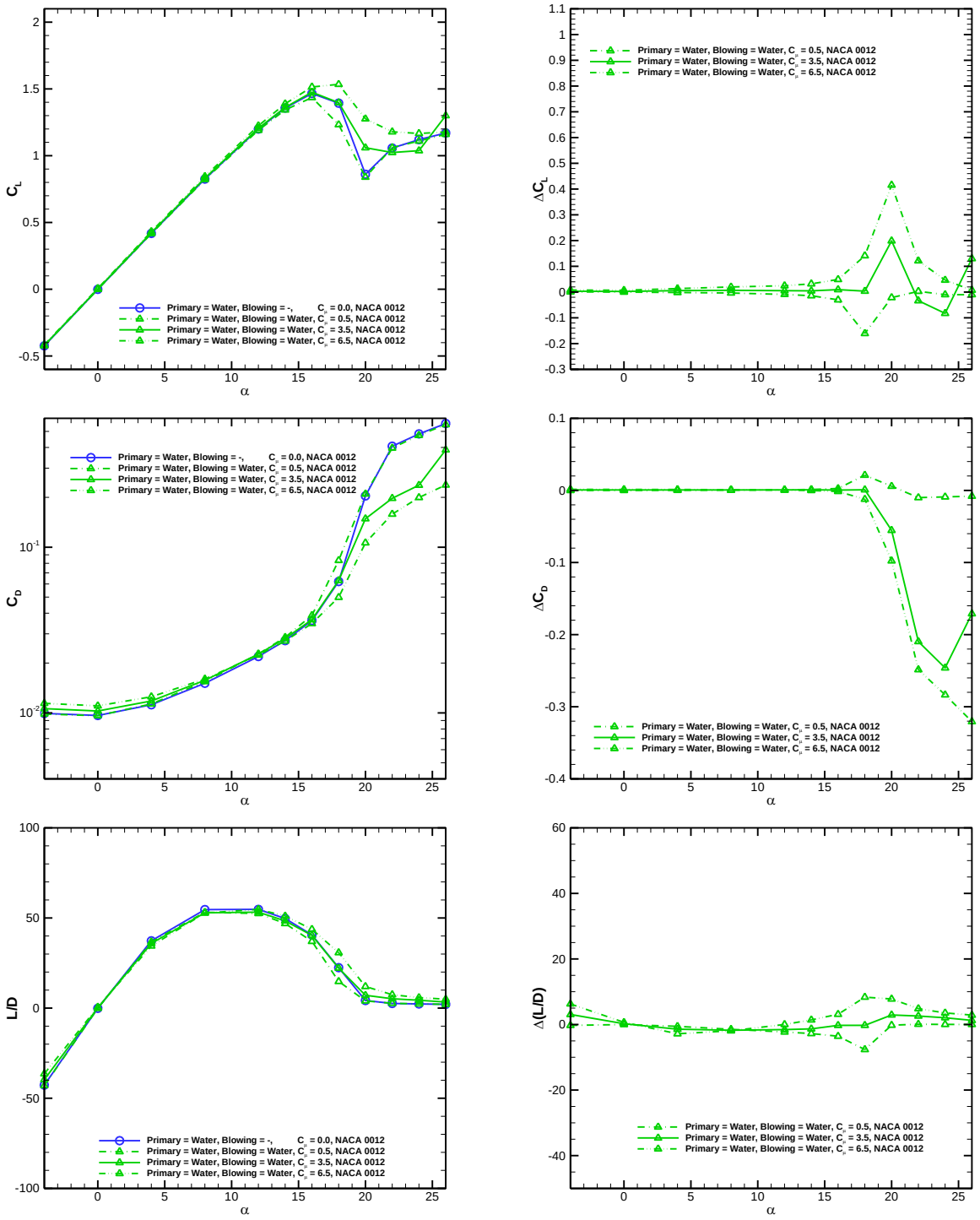


Fig. 13 Effect of the water fluid bellowing at different momentum coefficients on the performance of NACA 0012.

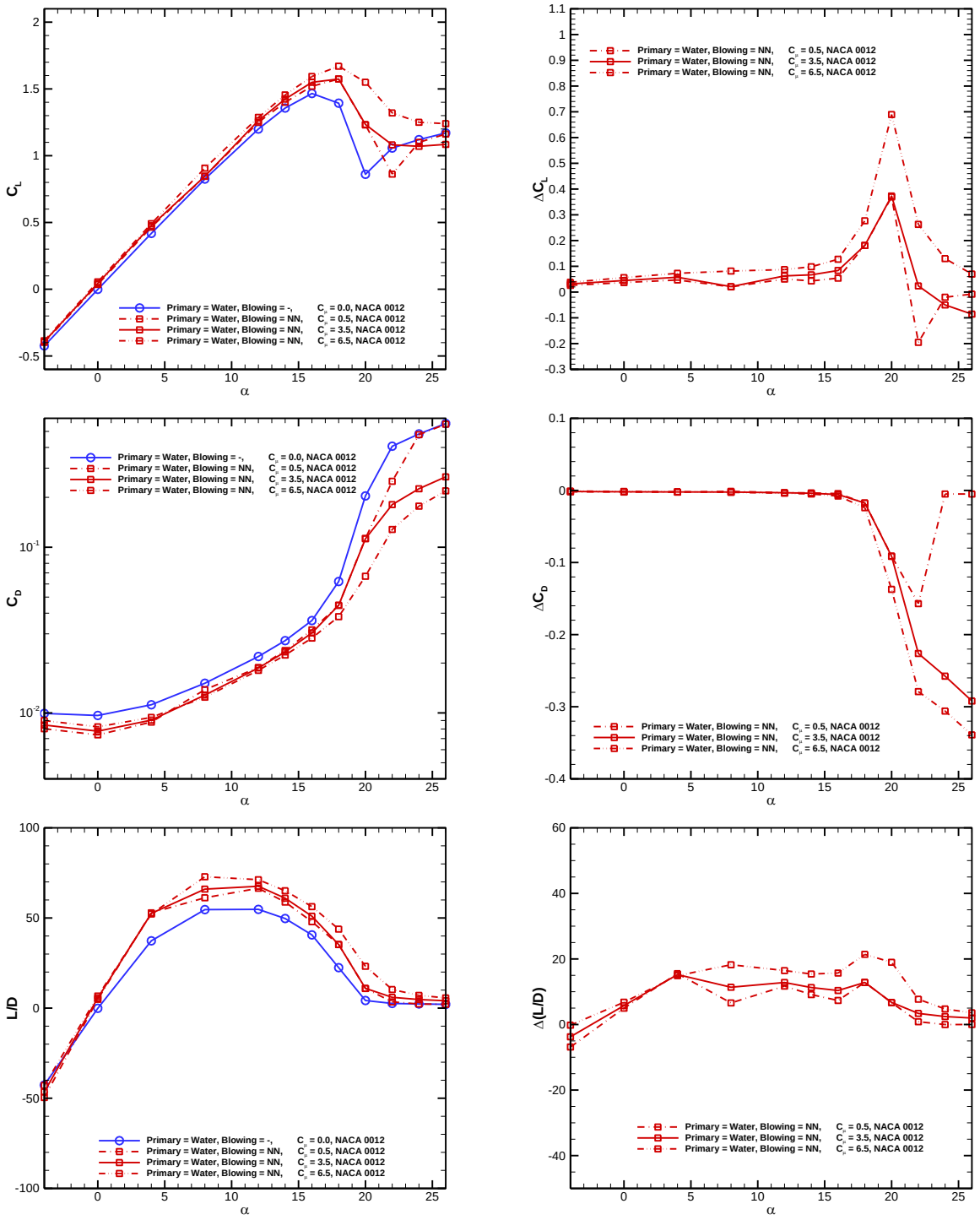


Fig. 14 Effect of the NN fluid bellowing at different momentum coefficients on the performance of NACA 0012.

### 5.4. Effect of the change of the non-Newtonian fluid from the Carreau to the Prandtl-Eyring fluid

In Sections 5.2 and 5.3, the non-Newtonian (NN) Carreau fluid was used, but here we are trying to figure out how changing the type of NN fluid from the Carreau to Prandtl-Eyring one may affect the results. Here, $C_\mu = 6.5$ is used which is the best configuration, among other values investigated, when we are seeking higher hydrofoil performance. In Fig. 15, the results obtained by employing the Prandtl-Eyring NN fluid are shown and they can be compared against the results for the Carreau presented in Fig. 11. The comparison shows that there is no significant change in the fluid flow structures.

The distribution of the volume fraction of the NN fluid on the suction side of the hydrofoil is illustrated in Fig. 16. As depicted in this figure, at $\alpha = 18^\circ$ the upper surface of the hydrofoil is almost covered by the pure NN fluid except near the leading edge where there is pure water and near the trailing edge where there is a mixture of the water-NN fluid. However, at $\alpha = 26^\circ$, the fluid flow tends to separate from the leading edge and the extra momentum injected into the boundary layer is not enough to maintain the flow attached and the fluid flow separates at a point close to the position of the slot. Although this is true for both NN fluids, using the NN Prandtl-Eyring fluid instead of the Carreau one favorably results in a little movement in the flow separation point toward the trailing edge.

The hydrodynamic parameters presented in Fig. 17 show that using the NN Prandtl-Eyring fluid is preferred in comparison with the Carreau one because it can produce higher lift coefficients, lower drag coefficients, and higher lift-to-drag ratio.

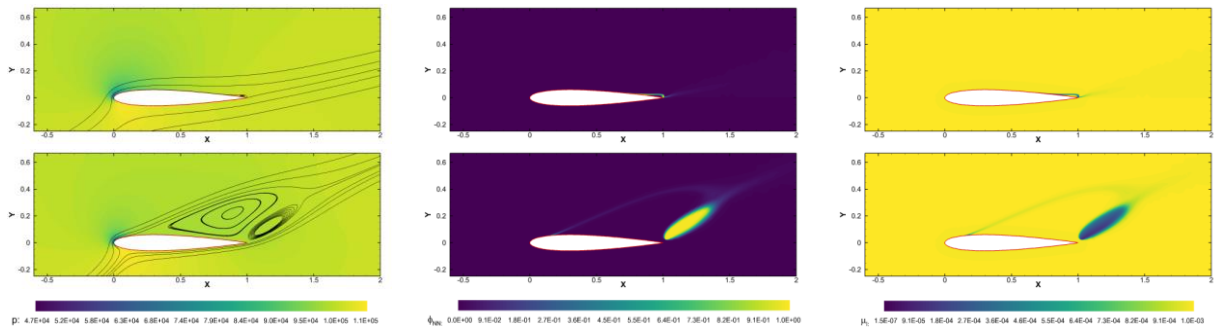

Fig. 15 Pressure contours with streamlines (left column), volume fraction contours of the NN Prandtl-Eyring fluid (middle column), and laminar viscosity coefficient contours (right column) obtained for the fluid flow past NACA 0012 hydrofoil at the momentum coefficient 6.5 and angles of attack $18^\circ$ (upper row) and $26^\circ$ (lower row).

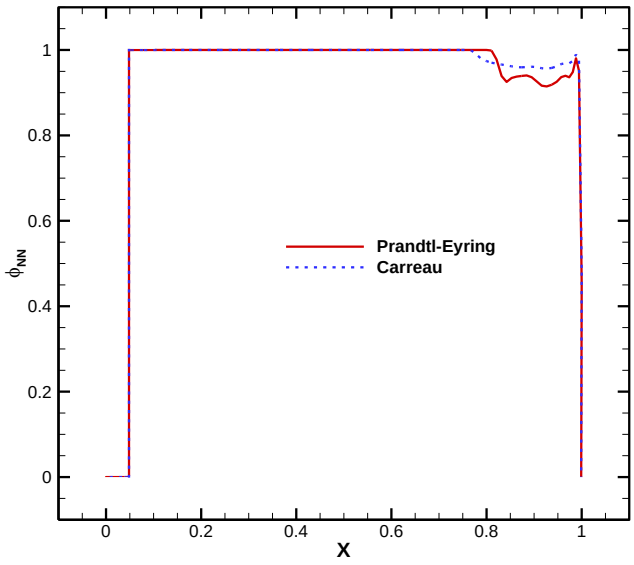


(a)

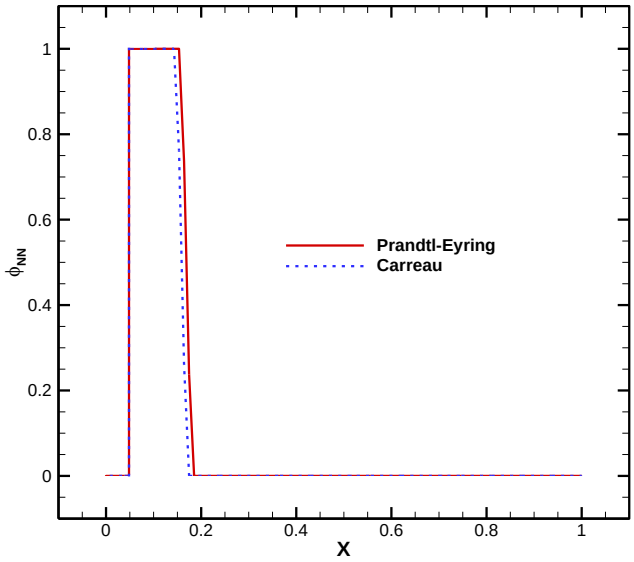


(b)

Fig. 16 Effect of the type of the injecting NN fluid over NACA 0012 on the surface volume fraction at the angles of attack a) $18^{\circ}$ and b) $26^{\circ}$.

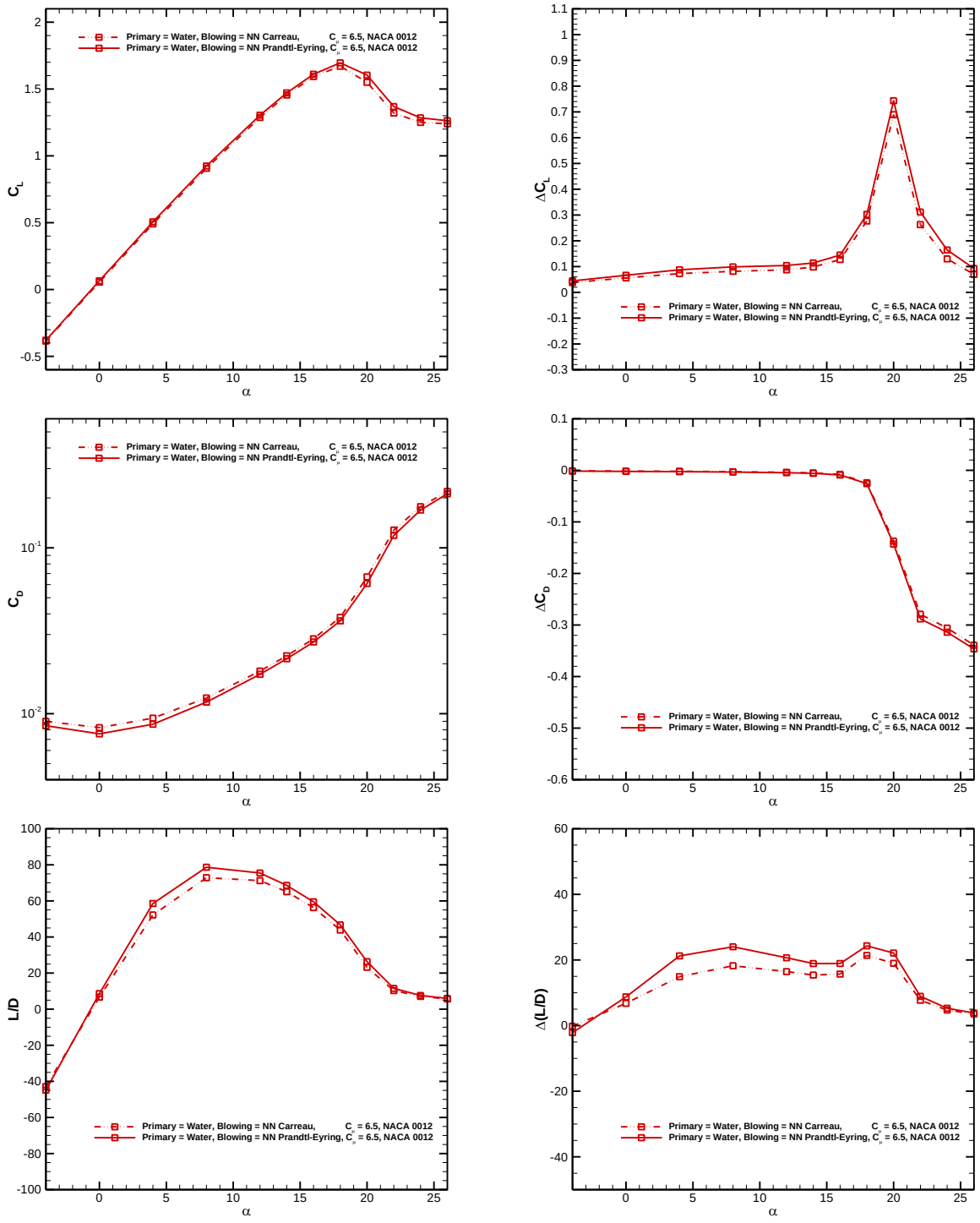


Fig. 17 Effect of the type of the injecting NN fluid over NACA 0012 on the performance of this hydrofoil.

### 5.5. Effect of the change of the hydrofoil from NACA 0012 to NACA 0018

In this section, we are going to figure out if the idea of using non-Newtonian fluids for actively controlling the flow characteristics and improving the hydrofoil performance is still acceptable for a thicker hydrofoil like NACA 0018.

#### 5.5.1. Effect of the type of the injecting fluid for NACA 0018

While in Sections 5.2-5.4 only NACA 0012 hydrofoil was used in simulations, here the hydrodynamic performance of NACA 0018 will be investigated. This hydrofoil is produced by scaling up NACA 0012 in the $y$-direction, so that the number of grid points and the location of the slot remain unchanged. Here, $C_\mu = 6.5$ is used which is the ideal case with the best output performance in our study. Flow characteristics obtained are shown in Fig. 18 showing that there is a smaller separated flow region over NACA 0018 in comparison with NACA 0012 presented in Fig. 11, but generally, flow-fields look similar. The hydrodynamic parameters are also illustrated in Fig. 19. Results show that when the water injects through the slot, the lift coefficient will dramatically increase. But, the drag coefficient at low/moderate angles of attack can be higher than the case of the without injection, however, it desirably becomes lower at high angles of attack. Subsequently, the lift-to-drag ratio will be higher than the case of the without injection if the water blows at high angles of attack. However, by utilizing the NN fluid better hydrofoil performance will be obtained including lower drag and higher lift coefficients. Note that, the lift coefficient is still much higher when the NN fluid is used rather than the water one. Therefore, the NN fluid can be preferred to the water in all the range of angles of attack.

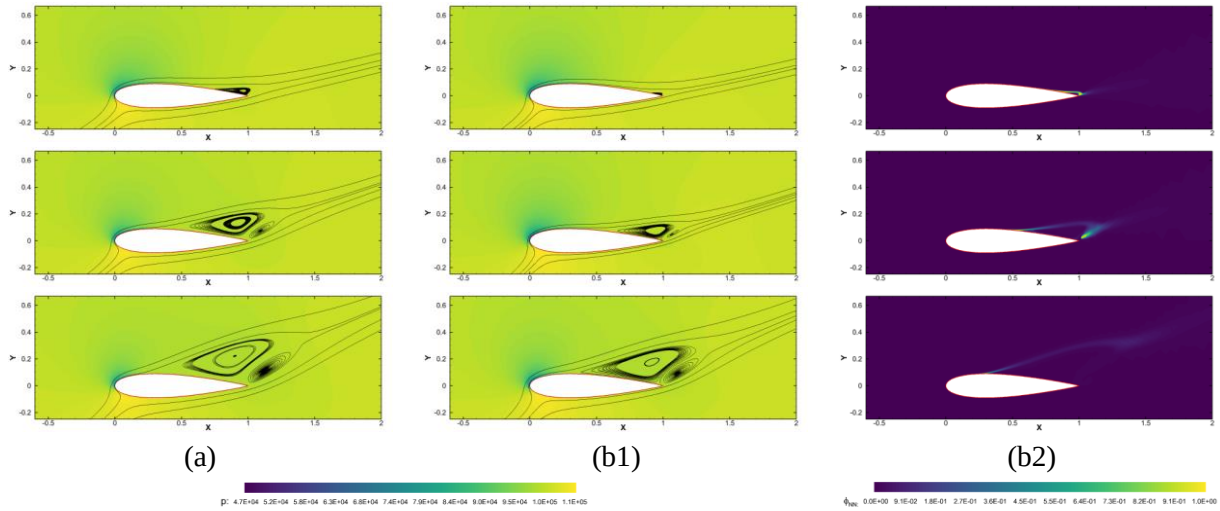


Fig. 18 Pressure contours with streamlines and volume fraction contours obtained for the injection of a) the water and b) NN fluid over NACA 0018 hydrofoil at the momentum coefficient 6.5 and angles of attack $18^\circ$ (upper row), $22^\circ$ (middle row), and $26^\circ$ (lower row).

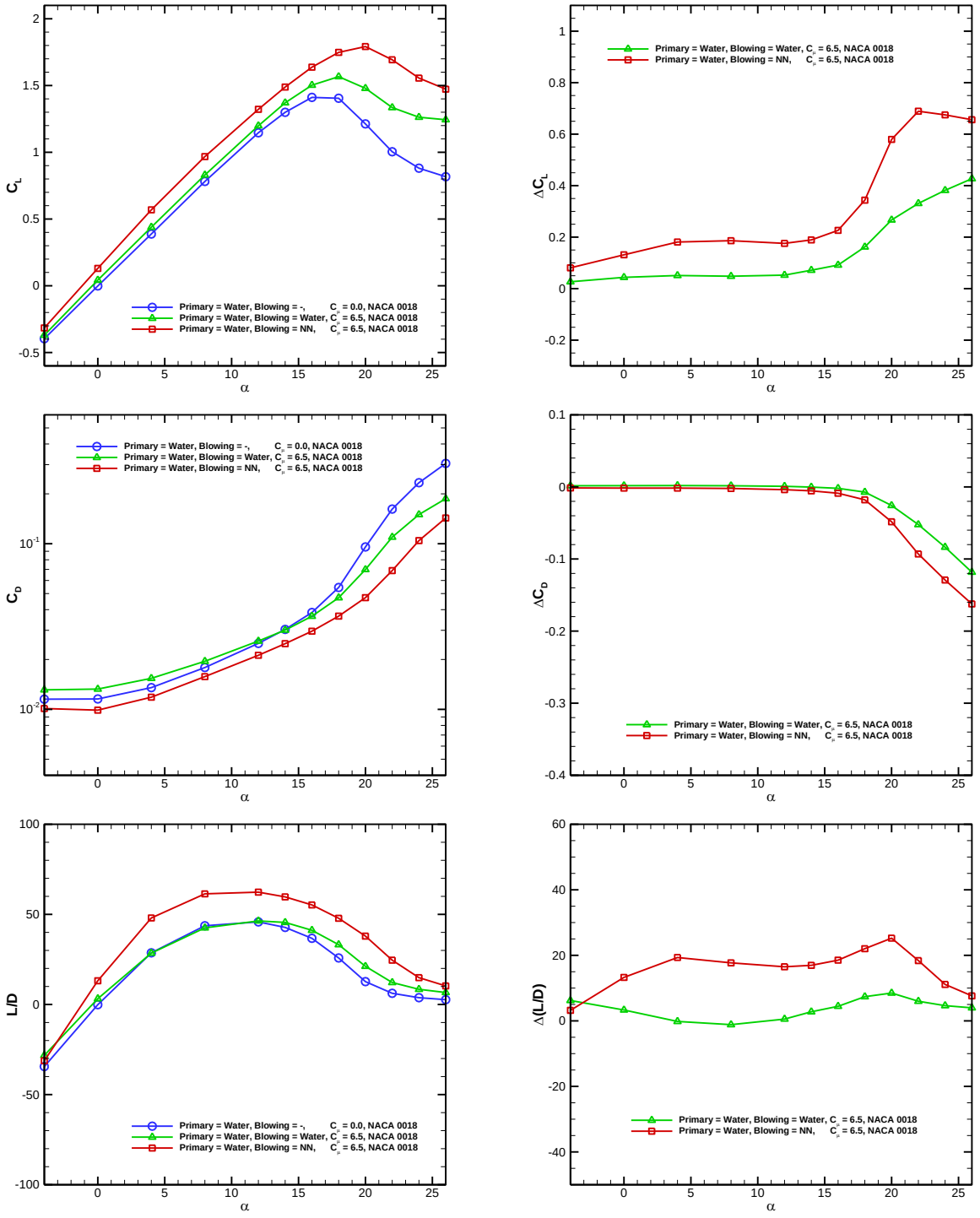


Fig. 19 Performance of NACA 0018 calculated at the momentum coefficient 6.5.

### 5.5.2. Effect of the hydrofoil thickness

The comparison between the hydrodynamic performance of NACA 0018 and NACA 0012 is shown in Fig. 20 and it can be seen that NACA 0018 has higher lift coefficients in all the range of angles of attack, higher drag coefficient at low angles of attack, and lower drag coefficient at high angles of attack. As for NACA 0018, the lift coefficient is the parameter that improved dramatically, especially at high angles of attack. In the case of NACA 0012, this is the drag coefficient that is strongly affected by the injection of the NN fluid and it can be obviously seen that at high angles of attack the drag coefficient is significantly reduced. In general, although the injection has significant effects on the performance of both NACA 0012 and NACA 0018, it has a more impact on the hydrodynamic performance of NACA 0018, especially when we are looking at the lift-to-drag parameter.

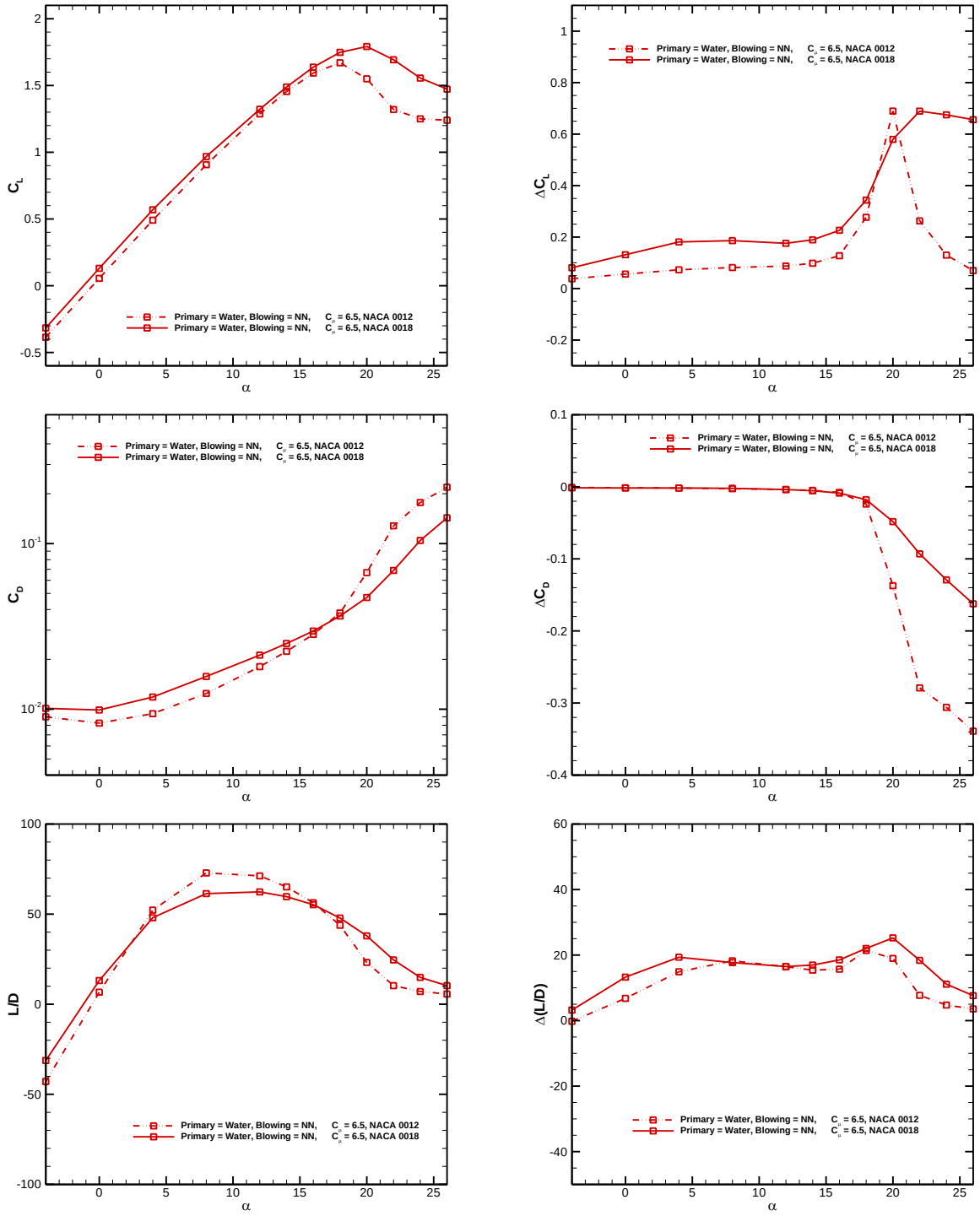


Fig. 20 Effect of the thickness of the hydrofoil on the hydrodynamic performance obtained when the NN fluid is injected over the upper surface.

## 6. Conclusion

In this study, an active flow control method by continuous injection of non-Newtonian (NN) fluids through a slot over hydrofoils is proposed and investigated. Different non-Newtonian fluids such as the power-law, Cross, Carreau, Ellis, and Prandtl-Eyring are discussed and among them, the Carreau and Prandtl-Eyring NN fluids are selected for more detailed studies.

The fluid flow is simulated by solving the two-phase Navier-Stokes equations using the finite volume and the implicit Euler methods to discretize the spatial and temporal derivative terms, respectively. Moreover, the Volume of Fluid (VoF) based method, especially the Compressive Interface Capturing Scheme for Arbitrary Meshes (CICSAM), is used to capture the interface between two fluids. The numerical solver has been examined for the solution of the turbulent flow past NACA 0012 and NACA 0018 hydrofoils and the agreement between numerical results obtained and the experimental data are satisfactory.

Then, without injection and by changing the surrounding/primary fluid, the effectiveness of the NN fluid serving as a surrounding fluid is investigated. In general, NACA 0012 operating in the NN fluid medium attains a better hydrodynamic performance, but the main improvement is expected near the stall point not far from that.

Flow-field characteristics and hydrodynamic performances are also investigated when the water and NN fluids are injected through a slot over the suction side of NACA 0012 hydrofoil. Three different momentum coefficients $C_m$ are studied in this study. Numerical results demonstrate that injection of the water with $C_m = 0.5$ will deteriorate the hydrofoil performance parameters. Although the injection of the water may cause the reduction in the lift-to-drag ratio for an angle of attack before the stall point, it will be helpful to use the injection of the water with $C_m = 6.5$ to improve the hydrofoil performance at high angles of attack. However, generally, the NN fluid will desirably always improve the hydrofoil performance parameters even for $C_m = 0.5$ and for all the range of angles of attack investigated in this study. Basically, using higher momentum coefficients is indeed helpful to delay the emergence of unsteady fluid flows and to prevent the boundary layer separation. Thus, using the NN fluid and higher momentum coefficients are always suggested.

The effect of the change of the NN fluid from the Carreau to the Prandtl-Eyring fluid is also investigated. Numerical results obtained in this study show that the fluid flow structures/patterns will not significantly change, however, the hydrofoil performance evaluated by the lift coefficient, drag coefficient, and lift-to-drag ratio will be improved. Therefore, the NN Prandtl-Eyring fluid is preferred to the Carreau one.

Changing the hydrofoil thickness is also studied here where the active flow control method based on the injection of the NN fluid is applied to improve the performance of NACA 0018 instead of NACA 0012. Results obtained show that this flow control method perfectly also works for thicker hydrofoil, even better than the thinner ones.

Results obtained in this study show that the proposed active flow control method based on the injection of the NN fluid can be considered as an alternative method to other flow control techniques to control flow characteristics and to significantly enhance the hydrofoil performance parameters.

## References


[1] R.-f. Huang, T.-z. Du, Y.-w. Wang, and C.-g. Huang, "Numerical investigations of the transient cavitating vortical flow structures over a flexible NACA66 hydrofoil," *Journal of Hydrodynamics,* vol. 32, no. 5, pp. 865-878, 2020.

[2] Z. Ni, M. Dhanak, and T.-c. Su, "Performance of a slotted hydrofoil operating close to a free surface over a range of angles of attack," *Ocean Engineering,* vol. 188, p. 106296, 2019.

[3] G. Sun, Y. Wang, Y. Xie, K. Lv, and R. Sheng, "Research on the effect of a movable gurney flap on energy extraction of oscillating hydrofoil," *Energy,* vol. 225, p. 120206, 2021.

[4] F. Li, Q. Huang, G. Pan, and Y. Shi, "Effect of hydrofoil leading edge waviness on hydrodynamic performance and flow noise," *Ocean Engineering,* vol. 231, p. 108883, 2021.

[5] P. Kundu, "Effects of circular trailing edge with the dimple on flow separation of NACA S1210 hydrofoil," *Proceedings of the Institution of Mechanical Engineers, Part C: Journal of Mechanical Engineering Science,* vol. 234, no. 18, pp. 3600-3613, 2020.

[6] Q. Wei, H.-x. Chen, and R. Zhang, "Numerical research on the performances of slot hydrofoil," *Journal of Hydrodynamics, Ser. B,* vol. 27, no. 1, pp. 105-111, 2015.

[7] B. Che and D. Wu, "Study on Vortex Generators for Control of Attached Cavitation," presented at the Proceeding of the ASME 2017 Fluids Engineering Division Summer Meeting. Volume 1A, Symposia: Keynotes; Advances in Numerical Modeling for Turbomachinery Flow Optimization; Fluid Machinery; Industrial and Environmental Applications of Fluid Mechanics; Pumping Machinery; Pumping Machinery, Waikoloa, Hawaii, USA, 2017.

[8] T. Sun, Z. Wang, L. Zou, and H. Wang, "Numerical investigation of positive effects of ventilated cavitation around a NACA66 hydrofoil," *Ocean Engineering,* vol. 197, p. 106831, 2020.

[9] C.-S. Lee, B.-K. Ahn, J.-M. Han, and J.-H. Kim, "Propeller tip vortex cavitation control and induced noise suppression by water injection," *Journal of Marine Science and Technology,* vol. 23, no. 3, pp. 453-463, 2018.

[10] M. V. Timoshevskiy, I. I. Zapryagaev, K. S. Pervunin, and D. M. Markovich, "Cavitating flow control through continuous tangential mass injection on a 2D hydrofoil at a small attack angle," *MATEC Web Conf.,* vol. 84, 2016.

[11] W. Wang, Q. Yi, S. Lu, and X. Wang, "Exploration and Research of the Impact of Hydrofoil Surface Water Injection on Cavitation Suppression," 2017.

[12] W. Wang, Q. Zhang, T. Tang, S. Lu, Q. Yi, and X. Wang, "Numerical study of the impact of water injection holes arrangement on cavitation flow control," *Science Progress,* vol. 103, no. 1, p. 0036850419877742, 2019.

[13] W. Wang *et al.*, "Effect of water injection on the cavitation control:experiments on a NACA66 (MOD) hydrofoil," *Acta Mechanica Sinica,* vol. 36, no. 5, pp. 999-1017, 2020.

[14] P. Akbarzadeh and E. Akbarzadeh, "Hydrodynamic characteristics of blowing and suction on sheet-cavitating flows around hydrofoils," *Ocean Engineering,* vol. 114, pp. 25-36, 2016.

[15] M. G. De Giorgi, D. Fontanarosa, and A. Ficarella, "Active Control of Unsteady Cavitating Flows Over Hydrofoil," *Journal of Fluids Engineering,* vol. 142, no. 11, 2020.

[16] K. Watanabe and H. Udagawa, "Drag reduction of non-newtonian fluids in a circular pipe with a highly water-repellent wall," *AIChE Journal,* vol. 47, no. 2, pp. 256-262, 2001.

[17] B. E. Owolabi, D. J. C. Dennis, and R. J. Poole, "Turbulent drag reduction by polymer additives in parallel-shear flows," *Journal of Fluid Mechanics,* vol. 827, p. R4, 2017, Art. no. R4.

[18] E. Rasti, F. Talebi, and K. Mazaheri, "Improvement of drag reduction prediction in viscoelastic pipe flows using proper low-Reynolds k-ε turbulence models," *Physica A: Statistical Mechanics and its Applications,* vol. 516, pp. 412-422, 2019.

[19] G. L. Chahine, G. F. Frederick, and R. D. Bateman, "Propeller Tip Vortex Cavitation Suppression Using Selective Polymer Injection," *Journal of Fluids Engineering,* vol. 115, no. 3, pp. 497-503, 1993.
[20] R. I. Tanner and K. Walters, *Rheology: an historical perspective*. Elsevier, 1998.
[21] K. M. Gangawane and H. F. Oztop, "Mixed convection in the semi-circular lid-driven cavity with heated curved wall subjugated to constant heat flux for non-Newtonian power-law fluids," *International Communications in Heat and Mass Transfer,* vol. 114, p. 104563, 2020.
[22] M. M. Cross, "Rheology of non-Newtonian fluids: A new flow equation for pseudoplastic systems," *Journal of Colloid Science,* vol. 20, no. 5, pp. 417-437, 1965.
[23] F. A. R. Pereira, M. A. S. Barrozo, and C. H. Ataíde, "CFD predictions of drilling fluid velocity and pressure profiles in laminar helical flow," *Brazilian Journal of Chemical Engineering,* vol. 24, no. 4, pp. 587-595, 2007.
[24] R. B. Bird, R. C. Armstrong, and O. Hassager, "Dynamics of polymeric liquids. Vol. 1: Fluid mechanics," 1987.
[25] P. J. Carreau, "Rheological Equations from Molecular Network Theories," *Transactions of the Society of Rheology,* vol. 16, no. 1, pp. 99-127, 1972.
[26] T. Sochi, "Flow of non-newtonian fluids in porous media," *Journal of Polymer Science Part B: Polymer Physics,* vol. 48, no. 23, pp. 2437-2767, 2010.
[27] A. Lenci, S. Longo, and V. Di Federico, "Shear-Thinning Fluid Flow in Variable-Aperture Channels," *Water,* vol. 12, no. 4, 2020.
[28] J. Schenk and J. Van Laar, "Heat transfer in non-Newtonian laminar flow in tubes," *Applied Scientific Research, Section A,* vol. 7, no. 6, pp. 449-462, 1958.
[29] M. Hajihassanpour and K. Hejranfar, "A high-order nodal discontinuous Galerkin method to solve preconditioned multiphase Euler/Navier-Stokes equations for inviscid/viscous cavitating flows," *International Journal for Numerical Methods in Fluids,* vol. 92, no. 5, pp. 478-508, 2020.
[30] K. Hejranfar and M. Hajihassanpour, "A high-order nodal discontinuous Galerkin method for solution of compressible non-cavitating and cavitating flows," *Computers & Fluids,* vol. 156, pp. 175-199, 2017.
[31] O. Ubbink and R. I. Issa, "A Method for Capturing Sharp Fluid Interfaces on Arbitrary Meshes," *Journal of Computational Physics,* vol. 153, no. 1, pp. 26-50, 1999.
[32] T. Wacławczyk and T. Koronowicz, "Comparison of CICSAM and HRIC high-resolution schemes for interface capturing," *Journal of theoretical and applied mechanics,* vol. 46, pp. 325-345, 2008.
[33] P. Spalart and S. Allmaras, "A one-equation turbulence model for aerodynamic flows," in *30th Aerospace Sciences Meeting and Exhibit*(Aerospace Sciences Meetings: American Institute of Aeronautics and Astronautics, 1992.
[34] D. C. Eleni, T. I. Athanasios, and M. P. Dionissios, "Evaluation of the turbulence models for the simulation of the flow over a National Advisory Committee for Aeronautics (NACA) 0012 airfoil," *Journal of Mechanical Engineering Research,* vol. 4, no. 3, pp. 100-111, 2012.
[35] S. Rogers, F. Menter, P. Durbin, and N. Mansour, "A comparison of turbulence models in computing multi-element airfoil flows," in *32nd Aerospace Sciences Meeting and Exhibit*(Aerospace Sciences Meetings: American Institute of Aeronautics and Astronautics, 1994.
[36] A. Ahadi, P. E. Sullivan, and Z. Saghir, "Comparison of Numerical and Experimental Results over a NACA0025 Airfoil Undergoing Separation," *Fluid Mechanics Research International Journal,* vol. 2, no. 1, pp. 22-31, 2018.
[37] P. Kennedy and R. Zheng, *Flow analysis of injection molds*. Carl Hanser Verlag GmbH Co KG, 2013.

[38] H. F. Müller-Vahl, C. Strangfeld, C. N. Nayeri, C. O. Paschereit, and D. Greenblatt, "Control of Thick Airfoil, Deep Dynamic Stall Using Steady Blowing," *AIAA Journal,* vol. 53, no. 2, pp. 277-295, 2014.
[39] I. H. Abbott and A. E. Von Doenhoff, *Theory of wing sections: including a summary of airfoil data*. Courier Corporation, 2012.
[40] G. E. Hassan, A. Hassan, and M. E. Youssef, "Numerical investigation of medium range re number aerodynamics characteristics for NACA0018 airfoil," *CFD letters,* vol. 6, no. 4, pp. 175-187, 2014.
[41] E. N. Jacobs and A. Sherman, "Airfoil section characteristics as affected by variations of the Reynolds number," *NACA Technical Report,* vol. 586, pp. 227-267, 1937.